Received: 9 June 2021 | Revised: 19 November 2021 | Accepted: 25 November 2021

DOI: 10.1002/qj.4222

Quarterly Journal of the Royal Meteorological Society RMetS

RESEARCH ARTICLE

Long-term single-column model intercomparison of diurnal cycle of precipitation over midlatitude and tropical land

Shuaiqi Tang[1] | Shaocheng Xie[2] | Zhun Guo[3] | Song-You Hong[4] | Boualem Khouider[5] | Daniel Klocke[6] | Martin Köhler[7] | Myung-Seo Koo[8] | Phani Murali Krishna[9] | Vincent E. Larson[1,10] | Sungsu Park[11] | Paul A. Vaillancourt[12] | Yi-Chi Wang[13] | Jing Yang[12] | Chimene L. Daleu[14] | Cameron R. Homeyer[15] | Todd R. Jones[14] | Neelam Malap[9] | Roel Neggers[16] | Thara Prabhakaran[9] | Enver Ramirez[17] | Courtney Schumacher[18] | Cheng Tao[2] | Peter Bechtold[19] | Hsi-Yen Ma[2] | J. David Neelin[20] | Xubin Zeng[21]

[1]Pacific Northwest National Laboratory, Richland, Washington, USA

[2]Lawrence Livermore National Laboratory, Livermore, California, USA

[3]Climate Change Research Center, Institute of Atmospheric Physics, Chinese Academy of Sciences, Beijing, China

[4]NOAA/Earth System Research Laboratory and CIRES/University of Colorado, Boulder, Colorado, USA

[5]Department of Mathematics and Statistics, University of Victoria, Victoria, British Columbia, Canada

[6]Hans Ertel Centre for Weather Research, Deutscher Wetterdienst, Offenbach, Germany

[7]Deutscher Wetterdienst, Offenbach, Germany

[8]Korea Institute of Atmospheric Prediction Systems, Seoul, South Korea

[9]Indian Institute of Tropical Meteorology, Pune, India

[10]Department of Mathematical Sciences, University of Wisconsin-Milwaukee, Milwaukee, Wisconsin, USA

[11]School of Earth and Environmental Sciences, Seoul National University, Seoul, South Korea

[12]Meteorology Research Division, Environment and Climate Change Canada, Dorval, Québec, Canada

[13]Research Center for Environmental Changes, Academia Sinica, Taipei, Taiwan

Abstract

General Circulation Models (GCMs) have for decades exhibited difficulties in modelling the diurnal cycle of precipitation (DCP). This issue can be related to inappropriate representation of the processes controlling sub-diurnal phenomena like convection. In this study, 11 single-column versions of GCMs are used to investigate the interactions between convection and environmental conditions, processes that control nocturnal convections, and the transition from shallow to deep convection on a diurnal time-scale. Long-term simulations are performed over two continental land sites: the Southern Great Plains (SGP) in the USA for 12 summer months from 2004 to 2015 and the Manacapuru site at the central Amazon (MAO) in Brazil for two full years from 2014 to 2015. The analysis is done on two regimes: afternoon convective regime and nocturnal precipitation regime. Most models produce afternoon precipitation too early, likely due to the missing transition of shallow-to-deep convection in these models. At SGP, the unified convection schemes better simulate the onset time of precipitation. At MAO, models produce the heating peak in a much lower level compared with observation, indicating too shallow convection in the models. For nocturnal precipitation, models that produce most of nocturnal precipitation all allow convection to be triggered above the boundary layer. This indicates the importance of model capability to detect elevated convection for simulating nocturnal precipitation. Sensitivity studies indicate that (a) nudging environmental variables towards observations has a minor impact on DCP, (b) unified treatment of shallow and deep convection and the capability to capture mid-level convection can help models better capture DCP, and (c) the interactions of the atmosphere with other components in the climate system (e.g. land) are also important for DCP simulations in coupled models. These results provide long-term statistical

[14]Department of Meteorology, University of Reading, Reading, UK

[15]School of Meteorology, University of Oklahoma, Norman, Oklahoma, USA

[16]Institute of Geophysics and Meteorology, University of Cologne, Cologne, Germany

[17]Numerical Modeling and Development Division, Center for Weather Forecasting and Climate Studies, National Institute for Space Research, São Paulo, Brazil

[18]Department of Atmospheric Sciences, Texas A&M University, College Station, Texas, USA

[19]European Centre for Medium-Range Weather Forecasts, Reading, UK

[20]Department of Atmospheric and Oceanic Sciences, University of California in Los Angeles, Los Angeles, California, USA

[21]Department of Hydrology and Atmospheric Sciences, University of Arizona, Tucson, Arizona, USA

Correspondence
S. Xie, Lawrence Livermore National Laboratory, Livermore, CA, 94551, USA.
Email: xie2@llnl.gov

Present Address
Daniel Klocke, Max-Planck-Institut für Meteorologie, Hamburg, Germany

Funding information
National Science Foundation, Grant/Award Number: AGS-1936810; U.S. Department of Energy, Office of Science, Grant/Award Numbers: SCW1655, SCW0783

insights on which physical processes are essential in climate models to simulate DCP.

KEYWORDS

3. Physical phenomenon, convection, diurnal cycle of precipitation, single-column model

1 | INTRODUCTION

The diurnal cycle of precipitation (DCP) is one of the most important signals affecting climate variability and weather forecasting. Although it is dominated by diurnal variation of solar insolation that greatly affects the surface energy budget and regulates surface temperature (Dai *et al.*, 1999), mesoscale propagating systems and large-scale envelopes are also responsible for regulating DCP (e.g. Rutledge and Hobbs, 1984; Wei *et al.*, 2020). As a benchmark for evaluating climate models (Covey *et al.*, 2016), DCP provides an excellent measure of how well climate models simulate not only the total amount of precipitation but also its frequency, intensity, timing and duration (Trenberth *et al.*, 2003).

General Circulation Models (GCMs) have for decades exhibited difficulties in modelling the diurnal precipitation. Dai (2006) examined 18 GCMs and found that many models showed peak precipitation around noontime over land and around 0200 local standard time (LST) over ocean, both a few hours earlier than observations. Covey *et al.* (2016) examined 24 models from phase 5 of the Coupled Model Intercomparison Project (CMIP5: Taylor *et al.*, 2012), and found similar biases; that is, GCMs produce warm-season rainfall too early in the day. Recently, Fiedler *et al.* (2020) and Tang *et al.* (2021) examined the

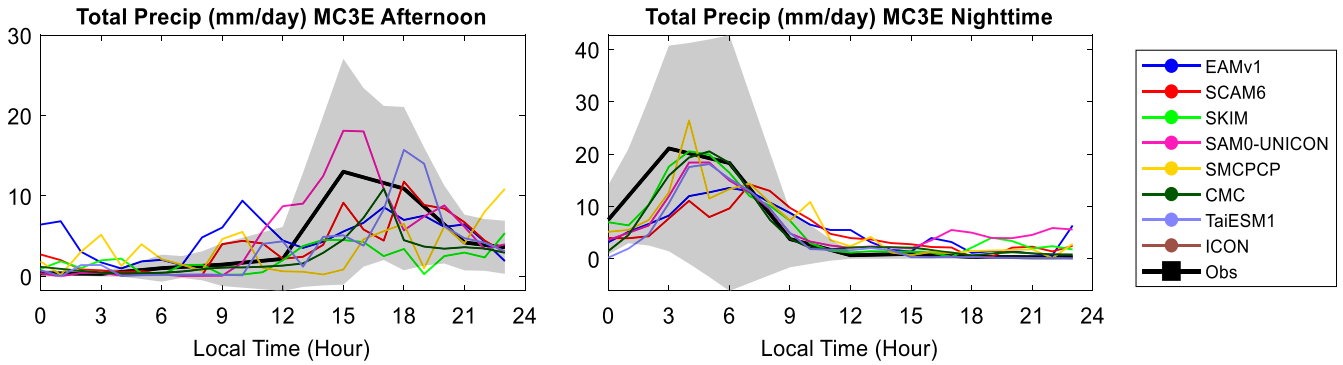

FIGURE 1 Diurnal cycle of total precipitation (mm·day^{-1}) averaged for the selected afternoon and nocturnal precipitation days during the MC3E field campaign

latest GCMs from CMIP6 (Eyring *et al.*, 2016) compared with earlier CMIP versions. They found that although CMIP6 models have made improvements on DCP, they still suffer from the same problems: producing rainfall too early in the day over land and missing the nocturnal rainfall peak associated with elevated convection and propagating mesoscale convective systems (MCSs).

These issues in simulating DCP in climate models can be related to inappropriate representation of the processes that control sub-diurnal phenomena like convection, and phenomena with time-scales of several hours, like MCSs. Many studies attribute the model biases in DCP to the deficiencies in convective parametrizations (e.g. Koo and Hong, 2010). Great efforts have been made to improve DCP in GCMs by improving the convective trigger (e.g. Xie and Zhang, 2000; Bechtold *et al.*, 2004; Rio *et al.*, 2009; Wang and Hsu, 2019; Xie *et al.*, 2019), closure (e.g. Zhang, 2003; Rio *et al.*, 2009; Bechtold *et al.*, 2014), entrainment and detrainment rates (e.g. Wang *et al.*, 2007; Bechtold *et al.*, 2008; Stratton and Stirling, 2012), or the detection of mid-level convection that is related to the nocturnal precipitation peak over regions such as the central USA (e.g. Lee *et al.*, 2008; Wang *et al.*, 2015; Xie *et al.*, 2019; McTaggart-Cowan *et al.*, 2020). Other parametrizations (e.g. Park, 2014a; 2014b; Neggers, 2015a; Guo *et al.*, 2021) that unify the deep convective scheme with other parametrizations also provide a path toward improving DCP simulation. One of the challenges is the difficulty to find parametric formulations that are valid for both shallow and deep convection (Del Genio, 2012), which have quite different underlying physical processes. Another challenge is understanding how the different physical processes evolve from one to the other, and how to represent them in models. This drives intense research into convective transitions, including various recent meteorological field campaigns dedicated to this problem, e.g. Cloud, Aerosol, and Complex Terrain Interactions (CACTI: Varble *et al.*, 2021).

A single-column model (SCM) is a useful tool to test physical processes within a column of a GCM (Randall *et al.*, 1996; Zhang *et al.*, 2016). In the past 20 years, several SCM intercomparison studies have been organized, focusing on summertime continental convection (Ghan *et al.*, 2000; Xie *et al.*, 2002; Guichard *et al.*, 2004), springtime midlatitude frontal clouds (Xie *et al.*, 2005; Xu *et al.*, 2005), shallow-cumulus clouds over midlatitude land (Lenderink *et al.*, 2004), marine stratocumulus-topped boundary layers (Bretherton *et al.*, 1999; Zhu *et al.*, 2005; Wyant *et al.*, 2007; Neggers *et al.*, 2017), mixed-phase clouds in the polar region (Klein *et al.*, 2009; Morrison *et al.*, 2009; Pithan *et al.*, 2016) and deep convection over the tropical ocean (Bechtold *et al.*, 2000; Davies *et al.*, 2013; Petch *et al.*, 2014). These intercomparison studies serve as testbeds for developing new parametrizations. For DCP, SCMs produce a similar diurnal structure of precipitation as the full three-dimensional (3-D) GCM and are thus suitable to be used as a simplified model of GCMs to explore the physical processes related to DCP (Betts and Jakob, 2002).

The above-mentioned SCM intercomparison studies mainly focused on case-studies. However, short-term simulations of a few days or a few weeks may not be long enough to build robust statistics for phenomena such as DCP since *a simulated diurnal peak may be determined by a few strong precipitation events and is largely controlled by the specified large-scale forcing*. For example, a 42-day simulation during the Midlatitude Continental Convective Clouds Experiment (MC3E: Jensen *et al.*, 2016) shows that most models in this study perform well on night-time precipitation (Figure 1), which is *inconsistent with what has been shown in their climate simulations* (e.g. Tang *et al.*, 2021*) and the findings from multi-year SCM simulations* shown later in this work (Section 3). In recent years efforts have been made to pursue longer-term SCM simulations at permanent meteorological sites (Neggers *et al.*, 2012). In certain conditions this allows direct

attribution of persistent biases in GCMs to parametrized subgrid-scale processes (Neggers and Siebesma, 2013; Neggers, 2015b). In the recent Global Atmospheric System Studies (GASS) Diurnal Cycle of Precipitation intercomparison project (https://portal.nersc.gov/project/capt/diurnal/), we are attempting to build robust statistics of the diurnal cycle of precipitation using long-term simulations from various weather and climate models. Two research sites from the Atmospheric Radiation Measurement (ARM) programme, Southern Great Plains (SGP) site in the central USA and the Manacapuru (MAO) site for the Green Ocean Amazon (GoAmazon2014/5: Martin *et al.*, 2016) experiment in Brazil, are chosen to build the long-term statistics of SCM performance. In addition, a few 1-day cases are selected to use both SCMs and cloud-resolving models (CRMs) for detailed process understanding of model errors in DCP. The goal of this study is to document common model behaviours in simulating the diurnal cycle of precipitation in current weather and climate models by constraining the large-scale conditions in the SCM framework and to provide a benchmark for more in-depth follow-up studies. In particular, this article will focus on the long-term statistics of the SCM simulations on DCP. More results on SCMs and CRMs for selected cases will be analysed in a separate article.

2 | EXPERIMENTAL DESIGN AND PARTICIPATING MODELS

2.1 | Experimental design

Two sets of SCM experiments are designed to build up statistics and connection to climate errors at two continental land locations using a series of short-range 5-day hindcast simulations. The first experiment spans 12 warm seasons (May–August) between 2004 and 2015 at the ARM SGP site. The second experiment is two full years from 2014 to 2015 at the ARM MAO site. The default protocol for the SCM simulations is a 5-day non-nudging hindcast, that is, each SCM is initiated at 0000 UTC every day and runs freely for 5 days without constraining temperature and moisture fields. Compared to typical SCM experiment protocols such as free run (e.g. Ghan *et al.*, 2000) or nudging run, in the 5-day hindcast run the large-scale condition will not drift too far away, and SCM is expected to replicate similar model biases as in GCM (Bogenschutz *et al.*, 2020), so that modellers can identify problems related to parametrizations using the SCM hindcast run. In this study, the 24–48 hr simulations (day-2 hindcast) are used for analysis. In total there are 123 days (1 May to 31 August) per warm season at SGP and 361 days (2 January to 28 December since the 5-day simulations do not cross 2 years) per year at MAO to build the statistics.

SCMs are driven with the large-scale forcing derived from the constrained variational analysis (Zhang and Lin, 1997; Zhang *et al.*, 2001), which has been widely used in earlier GASS SCM intercomparison studies. The large-scale forcing data at SGP are from the ARM continuous forcing datasets at SGP (Xie *et al.*, 2004; Tang *et al.*, 2019), while the large-scale forcing at MAO are described in Tang *et al.* (2016). The initial conditions, surface latent and sensible heat fluxes, horizontal winds and the large-scale horizontal and vertical advections are all prescribed from the large-scale forcing data. Precipitation in the large-scale forcing data, which are from radar measurements averaged within a domain of ∼300 km in diameter at SGP and ∼220 km in diameter at MAO, is also used to evaluate model performance.

2.2 | Participating models

Participants in this intercomparison project submitted results from 11 SCMs with all required simulations at SGP and MAO. The basic information of these models is listed in Table 1, and more information about their deep convective parametrizations is listed in Table 2. Note that some of these models have an inheritance relationship with differences in model versions or physical parametrizations. For example, EAMv1 has two other versions: EAMv1.trigger and EAMv1.SILHS, with different deep convective schemes. EAMv1.trigger applies a modified convective trigger that was shown to significantly improve DCP (Xie *et al.*, 2019); EAMv1.SILHS shuts off EAMv1's native deep convective scheme and lets the Cloud Layers Unified By Binormals scheme (CLUBB) treat both shallow and deep convection (Thayer-Calder *et al.*, 2015; Guo *et al.*, 2021), with a Subgrid Importance Latin Hypercube Sampler (SILHS: Larson and Schanen, 2013) to interface clouds with microphysics on the subgrid scale. Moreover, SCAM5 is the earlier version of SCAM6, and SAM0-UNICON is developed based on SCAM5 with a unified convection scheme (UNICON: Park, 2014a; 2014b) for shallow and deep convection. Some models also perform simulations with different model set-ups or configurations for sensitivity studies. For example, SCAM6 and SKIM perform simulations with an interactive land model; SKIM submitted simulations with atmospheric states nudging to the observations. The variety of simulations allows us to test model sensitivity to parametrizations and model set-up. Although models have different vertical and temporal resolution, they are all interpolated (or averaged)

TABLE 1 Participating models and their basic information

Model name	Full name	Vertical levels	Time step	Turbulence	Stratiform clouds	Shallow convection	References	Contact person
EAMv1	The E3SM[a] atmospheric model V1	72	30 min	CLUBB	MG2, CLUBB	CLUBB	Rasch *et al.* (2019); Bogenschutz *et al.* (2020)	Shaocheng Xie, Shuaiqi Tang
EAMv1.trigger[b]	EAMv1 with revised convective trigger	72	30 min	CLUBB	MG2, CLUBB	CLUBB	Xie *et al.* (2019)	Shaocheng Xie, Shuaiqi Tang
EAMv1.SILHS	EAMv1 with CLUBB-SILHS	72	30 min	CLUBB	MG2, CLUBB-SILHS	CLUBB-SILHS	Guo *et al.* (2021)	Vincent Larson, Zhun Guo
SCAM6	Single-column atmosphere model version 6	32	20 min	CLUBB	MG2, CLUBB	CLUBB	Gettelman *et al.* (2019)	Shuaiqi Tang
SCAM5	Single-column atmosphere model version 5	30	20 min	UW-diag_TKE	MG, Park1	UW-PB09	Neale *et al.* (2012)	Shuaiqi Tang
SAM0-UNICON	Seoul National University atmosphere model	30	20 min	UW-diag_TKE	MG, Park2	UNICON	Park *et al.* (2019)	Sungsu Park, Jihoon Shin
SKIM	Single-column Korean integrated model	64	10 min	Shin–Hong	WSM5, PCH16	HanPan	Hong *et al.* (2013); Hong *et al.* (2018)	Myung-Seo Koo, Song-you Hong
CMC	Canadian Meteorological Centre	84	450 s	TKE1.5	Sundqvist	M-Bechtold	McTaggart-Cowan *et al.* (2019a)	Paul Vaillancourt, Jing Yang
SMCPCP	Stochastic MultiCloud plume convective parametrization	30	20 min	HB	MG, Park1	Unified stochastic plume-ZM	Khouider and Leclerc (2019)	Boualem Khouider, Phani Murali Krishna
TaiESM1	Taiwan Earth system model version 1	30	30 min	UW-diag_TKE	MG, GTS	UW-PB09	Lee *et al.* (2020)	Yi-Chi Wang
ICON	Icosahedral non-hydrostatic weather and climate model	90	2 min	Raschendorfer00	Seifert08, Köhler20	Bechtold14	Zängl *et al.* (2015); Bašták Ďurán *et al.* (2021)	Martin Köhler, Daniel Klocke

[a] The full names and references of the acronyms and physical schemes are given in the Appendix.
[b] The results of EAMv1.trigger, EAMv1.SILHS and SCAM5 are only shown in the sensitivity studies in Section 4.

TABLE 2 Deep convective parametrizations in the participating SCMs

Model name	Deep convection	Closure	Convective trigger	Downdraught	Reference
EAMv1	Zhang–McFarlane scheme (ZM)	Dilute CAPE	1 CAPE >70 J·kg^{-1} 2 The air parcel launch level is chosen within the boundary layer	Starts from updraught-top mass flux	Xie *et al.* (2018)
EAMv1.trigger	ZM with revised convective trigger	Dilute CAPE	1 CAPE >0 2 dCAPE >0 3 The air parcel launch level is chosen between the surface and 600 hPa	Same as EAMv1	Xie *et al.* (2019)
EAMv1.SILHS	CLUBB-SILHS	No explicit closure	Not needed	Rain evaporation effect fluxes	Thayer-Calder *et al.* (2015); Griffin and Larson (2016)
SCAM6	ZM	Dilute CAPE	1 CAPE >70 J·kg^{-1} 2 The air parcel launch level is chosen within the boundary layer	Downdraught starts from updraught-top mass flux	Gettelman *et al.* (2019)
SCAM5	ZM	Dilute CAPE	Same as SCAM6	Same as SCAM6	Neale *et al.* (2012)
SAM0-UNICON	UNICON	No explicit closure	Not needed	Downdraught generated from updraught	Park (2014a; 2014b)
SKIM	KSAS	Quasi-equilibrium closure considering boundary-layer forcing	1 $P_{parcel\_start} - P_{LFC} < P_{crit}(RH_{low})$ 2 $P_{LFC\_w/o\_ent} - P_{LFC\_w/\_ent} < 25$ hPa 3 CIN < -120 m^2·s^{-2} 4 Cloud depth >150 hPa 5 Cloud work function >0	Starts from the level of minimum moist static energy between LFC and 450 hPa	Han *et al.* (2020)
CMC	Modified Kain–Fritsch (KF) with a mid-level elevated convective scheme	CAPE	1 Mixed parcel from PBL lifted to LCL to which a temperature perturbation is added is buoyant 2 Cloud depth > 3,000 m	Initiated at level of free sink	Kain and Fritsch (1990; 1992); McTaggart-Cowan *et al.* (2020)
SMCPCP	Unified stochastic plume-ZM	Weighted kinetic energy and CAPE	Same as SCAM6	Same as SCAM6	Khouider and Leclerc (2019)
TaiESM1	ZM with revised convective trigger	Dilute CAPE	1 CAPE > 70 J·kg^{-1} 2 $P_{parcel\_start} - P_{LFC} < 150$ hPa 3 The air parcel launch level is chosen between the surface and 600 hPa	Same as SCAM6	Wang and Hsu (2019)
ICON	Bechtold14	CAPE	Entraining parcels starting with levels up to 350 hPa above the surface that must detect cloud layer thicker than 200 hPa.	Starts from level of free sinking (LFS) M(LFS) = −0.3 M (up,base)	Bechtold *et al.* (2014)

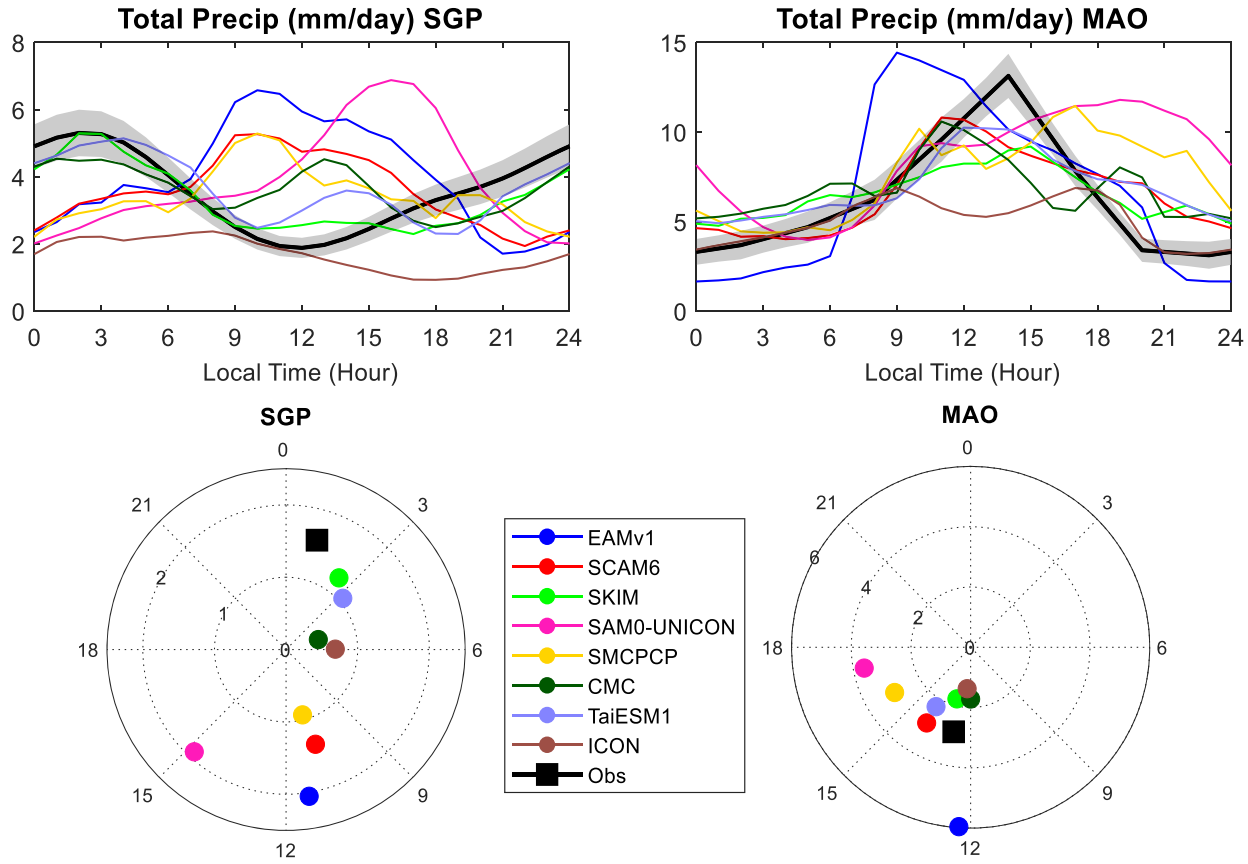

FIGURE 2 (top) The composite diurnal cycle time series and (bottom) the harmonic dial plots of total precipitation averaged for the long-term simulation periods at (left) SGP and (right) MAO. The grey shading in the time series indicates 1.96 × standard error (95% confidence) of the observed precipitation. The radius and phase of the harmonic dial plots represent the amplitude (mm·day^{-1}) and the peak hour (LST), respectively, of the first Fourier component of DCP

into 40 vertical levels and 1 hr resolution. The model data are archived and publicly available at https://portal.nersc.gov/project/mp193/GASS/SCM/data/.

3 | MODEL PERFORMANCES ON THE MEAN DIURNAL CYCLE OF PRECIPITATION

3.1 | General features

The two ARM sites are located in two distinct but representative environmental conditions: SGP represents typical midlatitude land condition with upper-level westerlies and dry free troposphere; MAO represents typical tropical rain-forest condition with warm, moist air in the lower and middle troposphere. A set of diagnostic plots of the meteorological and process-level variables are made available at the GASS-DCP quick-plot webpage (https://portal.nersc.gov/project/mp193/GASS/SCM/quick_plots/). Due to the length limit, this article only shows some of them that are closely related to DCP.

3.1.1 | Mean diurnal cycle of precipitation

The mean DCP and the harmonic dial plots for the 12 summer seasons at SGP and the 2 years at MAO are shown in Figure 2. "Harmonic dial plot" (Covey *et al.*, 2016) is a two-dimensional vector diagram in which the radius and angle represent the amplitude and phase, respectively, of the first component of Fourier analysis on the diurnal time series (sinusoidal function with period of 24 hr). The observed precipitation at SGP shows a nocturnal precipitation peak after midnight and a daytime minimum at around noon. The diurnal harmonic peak is at around 0100 LST. Many models, such as EAMv1, SCAM6, SAM0-UNICON and SMCPCP, produce a precipitation peak during daytime, with harmonic phases between ~1100 and 1500 LST and amplitudes between 1 and 2 mm·day^{-1}. The failure to produce a nocturnal precipitation peak at SGP is consistent with previous global model studies (e.g. Tang *et al.*, 2021). ICON produces an early-morning precipitation peak but its magnitude and diurnal amplitude are much lower than the observations. A few models produce a nocturnal precipitation peak,

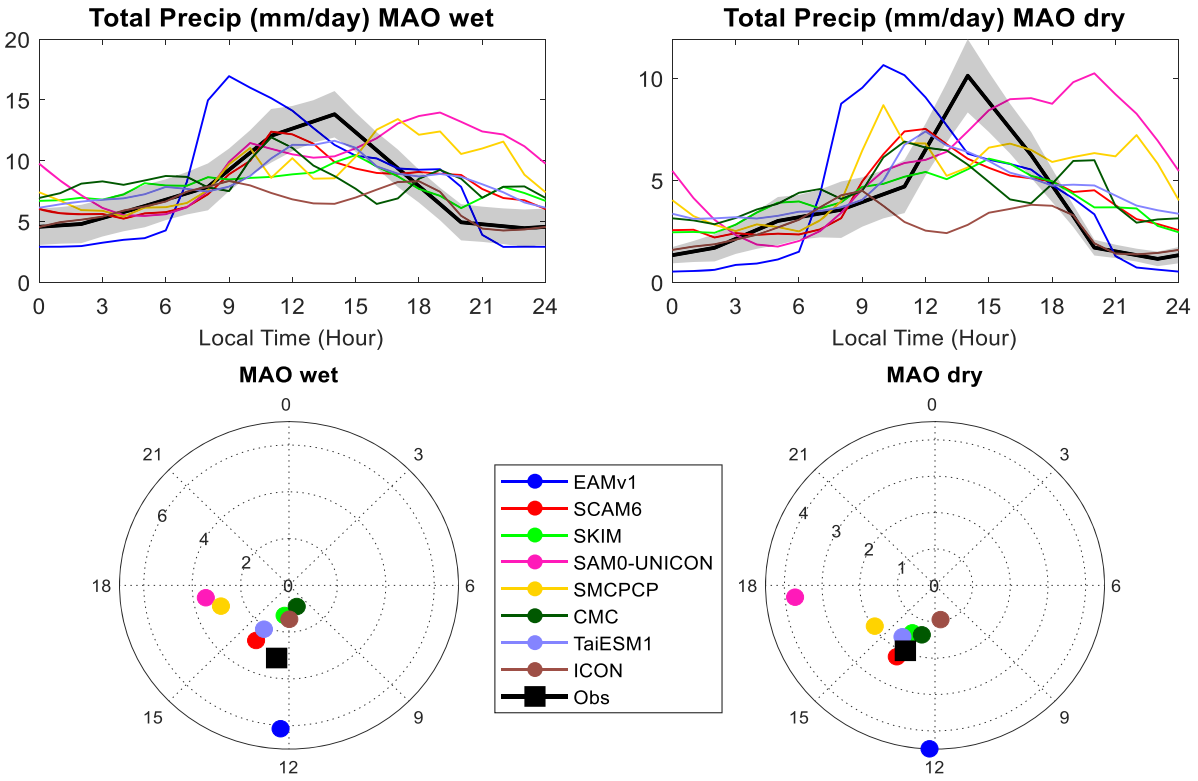

FIGURE 3 As in Figure 2 but for (left) wet season (December–March) and (right) dry season (July–October) at MAO

such as SKIM, CMC and TaiESM1. The mechanisms that help these models capture nocturnal precipitation will be discussed later in Section 3.3.

The observed precipitation at MAO shows an early afternoon peak with the diurnal harmonic peak just after noon. The precipitation peak is stronger and smoother in the wet season, while it is weaker and sharper in the dry season (Figure 3). Models have a spread in diurnal amplitude and phase, with precipitation amplitudes ranging from 1.5 to 6 mm·day^{-1} and the diurnal phases occurring as early as 1200 LST to as late as 1700 LST. The diurnal phases in both observations and models are more similar in the dry season than in the wet season, while the precipitation amounts and amplitudes are larger in the wet season in observation and most models (Figure 3). Since DCP is affected by several types of convective systems that occur at different times of the day in both dry and wet seasons (e.g. Tang *et al.*, 2016), we will focus on model performance for different types of convective systems instead of in different seasons.

3.1.2 | Diurnal cycle of clouds

The observed cloud fractions at SGP and MAO both show a low-level cloud peak rising along with the daytime boundary-layer development (Figure 4). The transition of shallow-to-deep convection has been extensively studied focusing on the following mechanisms: boundary-layer turbulence strength, including boundary-layer inhomogeneity (e.g. Zhang and Klein, 2010) and cold pools from rain evaporation (e.g. Khairoutdinov and Randall, 2006; Mapes and Neale, 2011; Del Genio *et al.*, 2012); and free-troposphere humidity and instability, including the preconditioning from shallow convection via detrainment or dilution (e.g. Rio *et al.*, 2009; Mapes and Neale, 2011; Del Genio *et al.*, 2012; de Rooy *et al.*, 2013; Hohenegger and Stevens, 2013; Ruppert and Johnson, 2015; Zermeño-Díaz *et al.*, 2015). Most of these studies used observations or idealized models, and only a few of them attempted to represent the transition in GCMs (Del Genio *et al.*, 2012; Rio *et al.*, 2013). Among the eight SCMs, SAM0-UNICON well captures the gradual rising of low clouds peak at both SGP and MAO; EAMv1 and SCAM6 capture the low clouds rising, although their low-cloud fraction is underestimated at SGP; other models all fail to produce the rising low clouds in the daytime. This result reveals that *capturing the development of shallow clouds and the transition from shallow to deep clouds is still a big challenge for current climate models. The encouraging results from using a unified scheme for turbulence and shallow convection (CLUBB) in EAMv1 and SCAM6 or a unified scheme for shallow and deep convection (UNICON) in SAM0-UNICON suggest the unified treatment of these processes could be one*

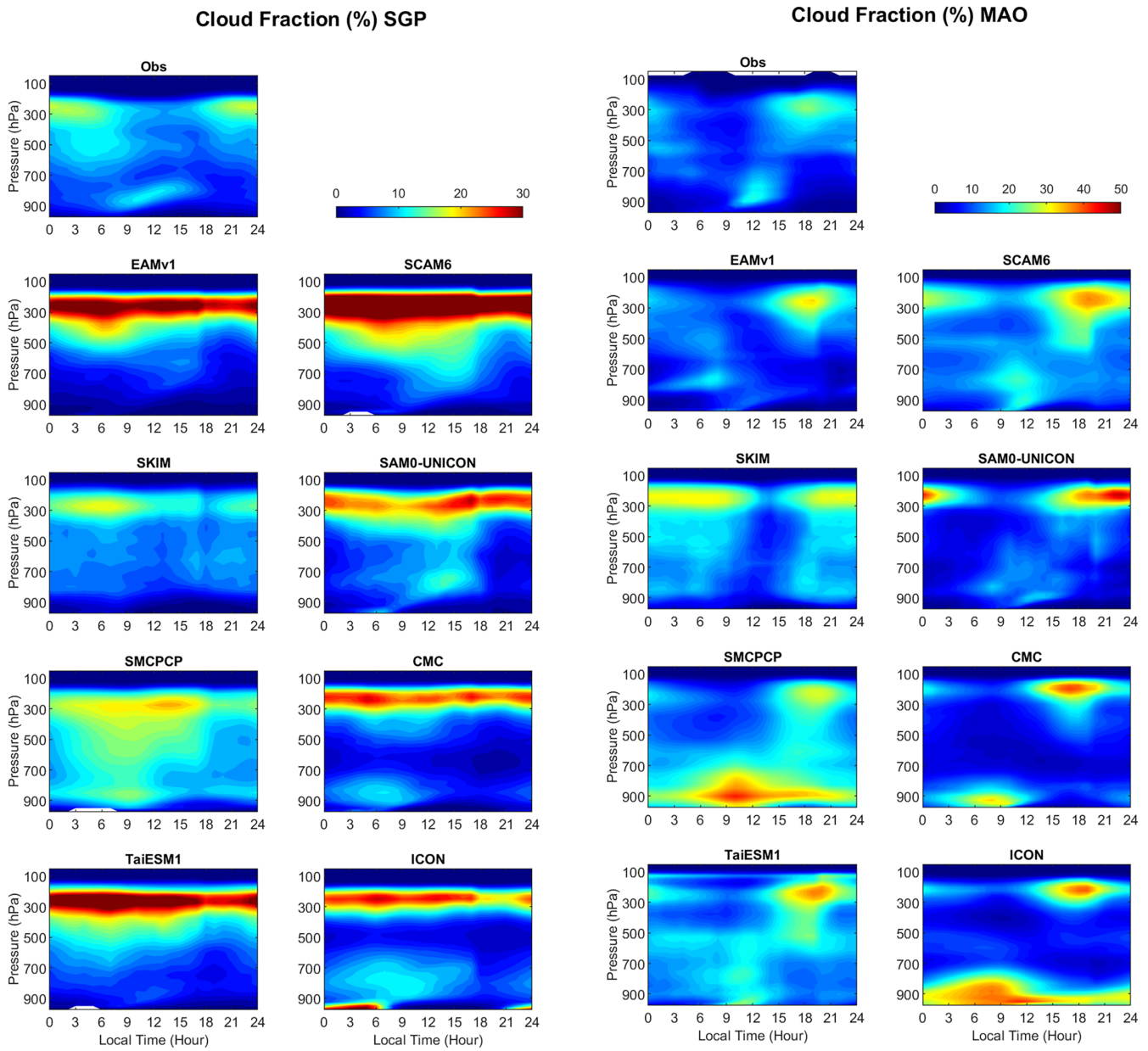

FIGURE 4 Diurnal cycle of cloud fraction (%) from observations and simulations at (left) SGP and (right) MAO

way to address this issue. This is consistent with the findings in previous attempts of unified schemes such as in Frenkel *et al.* (2011a; 2011b), which used a simple multicloud model coupled to a bulk boundary-layer scheme to simulate the diurnal cycle of tropical precipitation. For high clouds, most models overestimate high-cloud fraction compared to observations at SGP and MAO. The diurnal variation of high clouds is also poorly simulated at SGP but reasonably reproduced at MAO. Although model performances do behave differently at different locations, the differences of model–observation biases indicate the complexity of using one globally uniform parametrization to represent all environment conditions correctly.

3.1.3 | Precipitation versus relative humidity

Previous studies have shown a relationship between precipitation and column-integrated relative humidity (CRH) in observations at daily (e.g. Bretherton *et al.*, 2004) and sub-daily (e.g. Holloway and Neelin, 2009; Neelin *et al.*, 2009) time-scales, although it should be noted that using CRH is an approximation for a more complex precipitation–moisture–temperature relationship (Kuo *et al.*, 2018). How well models can capture the observed precipitation–CRH relationship is related to the representation of convection and its interaction with the large-scale environment, which provides insights to

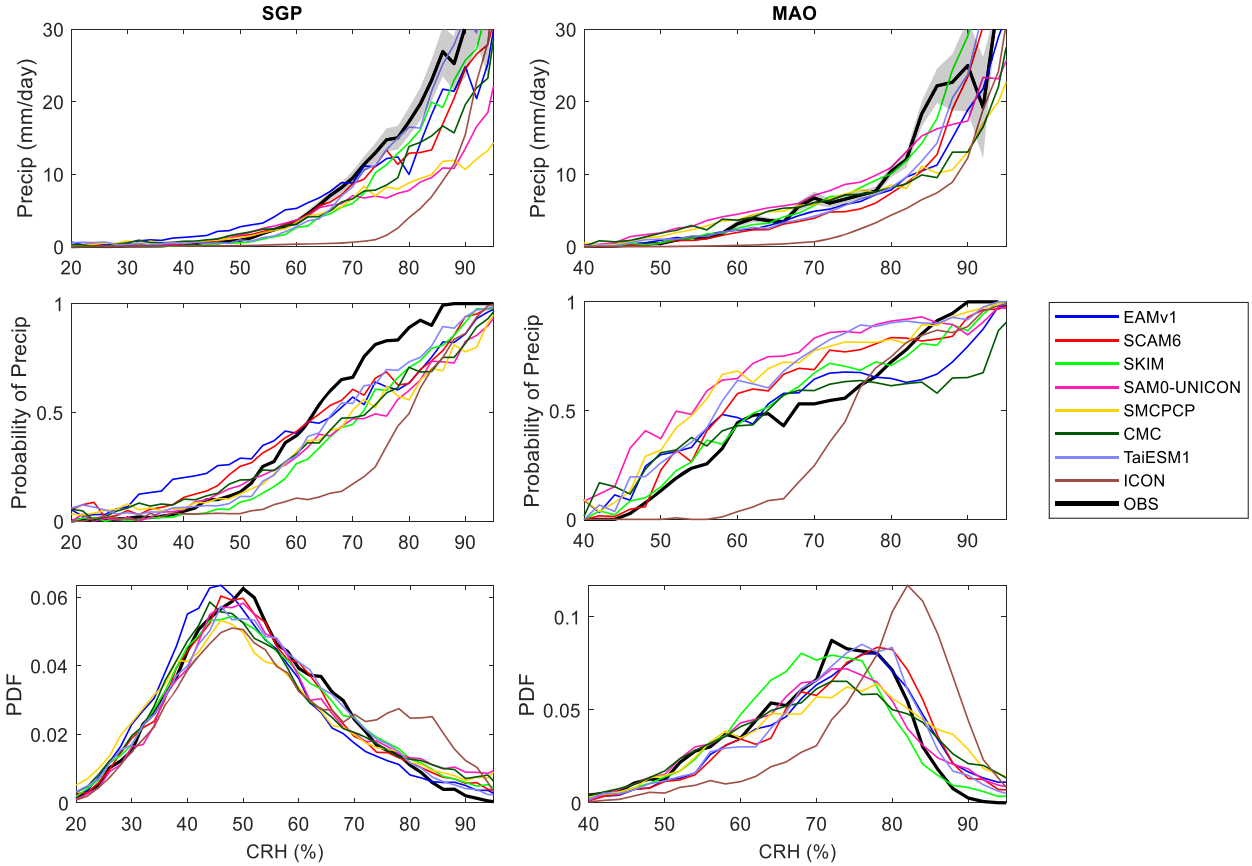

FIGURE 5 The relationship between precipitation and CRH for (left) SGP and (right) MAO: (top) the precipitation amount averaged for each CRH bin; (middle) the probability of precipitation exceeding 1 mm·day^{-1} for each CRH bin; (bottom) the occurrence frequency of each CRH bin. CRH is binned in intervals of 2%

model improvements on convection and precipitation (e.g. Kuo *et al.*, 2020). Here we examine the relationship of precipitation amount and frequency with CRH, as well as the occurrence frequency of each CRH bin (2% interval) in Figure 5. Observations show a strongly increasing relationship between precipitation amount and CRH at both sites. Precipitation picks up quickly and increases exponentially when CRH reaches 60%~70% at SGP and 75%~80% at MAO. Most models, except ICON, simulate higher (lower) precipitation probability (Figure 5, mid-row) and precipitation amount (Figure 5, top-row) compared to the observations when CRH is low (high). However, there are also more high-CRH days and fewer moderate-CRH days in these models than in observations (Figure 5, bottom-row). This indicates that models tend to produce light rainfall too easily in moderately dry conditions but have difficulties producing strong precipitation in wet conditions, although they are more likely to produce high CRH. This is consistent with the long-standing model error in GCMs that models rain too frequently at reduced intensity (Dai, 2006; Sun *et al.*, 2007; Stephens *et al.*, 2010). In ICON, precipitation picks up at a much higher CRH. It also produces more wet conditions and fewer dry conditions than observations and other models. This may be related to the fact that ICON requires the whole box to be saturated for large-scale precipitation while other models allow partial cloudiness for microphysics. This would lead to a later onset of large-scale precipitation and higher relative humidity in ICON.

In the next two subsections, we select two convection regimes to further investigate the model biases on DCP: afternoon precipitation regime that is primarily surface-driven deep convection and nocturnal precipitation regime that is primarily associated with propagating MCSs and elevated convection. Based on observations, the afternoon precipitation days are selected by modifying the criteria of Zhang and Klein (2010). For SGP, an afternoon precipitation day is chosen when it has (a) peak rain rate greater than 1 mm·day^{-1}, (b) rain peak time between 1300 and 2000 LST, and (c) the peak rain rate 1.5 times greater than any rain rate outside of 1300 to 2000 LST. For MAO, an afternoon precipitation day is chosen when it has (a) peak rain rate greater than 1 mm·day^{-1}, (b) rain peak time between 1100 and 2000 LST, (c) the peak rain rate 1.5 times greater than any rain rate outside of 1100 to 2000 LST, and (d) it must fall into the locally driven

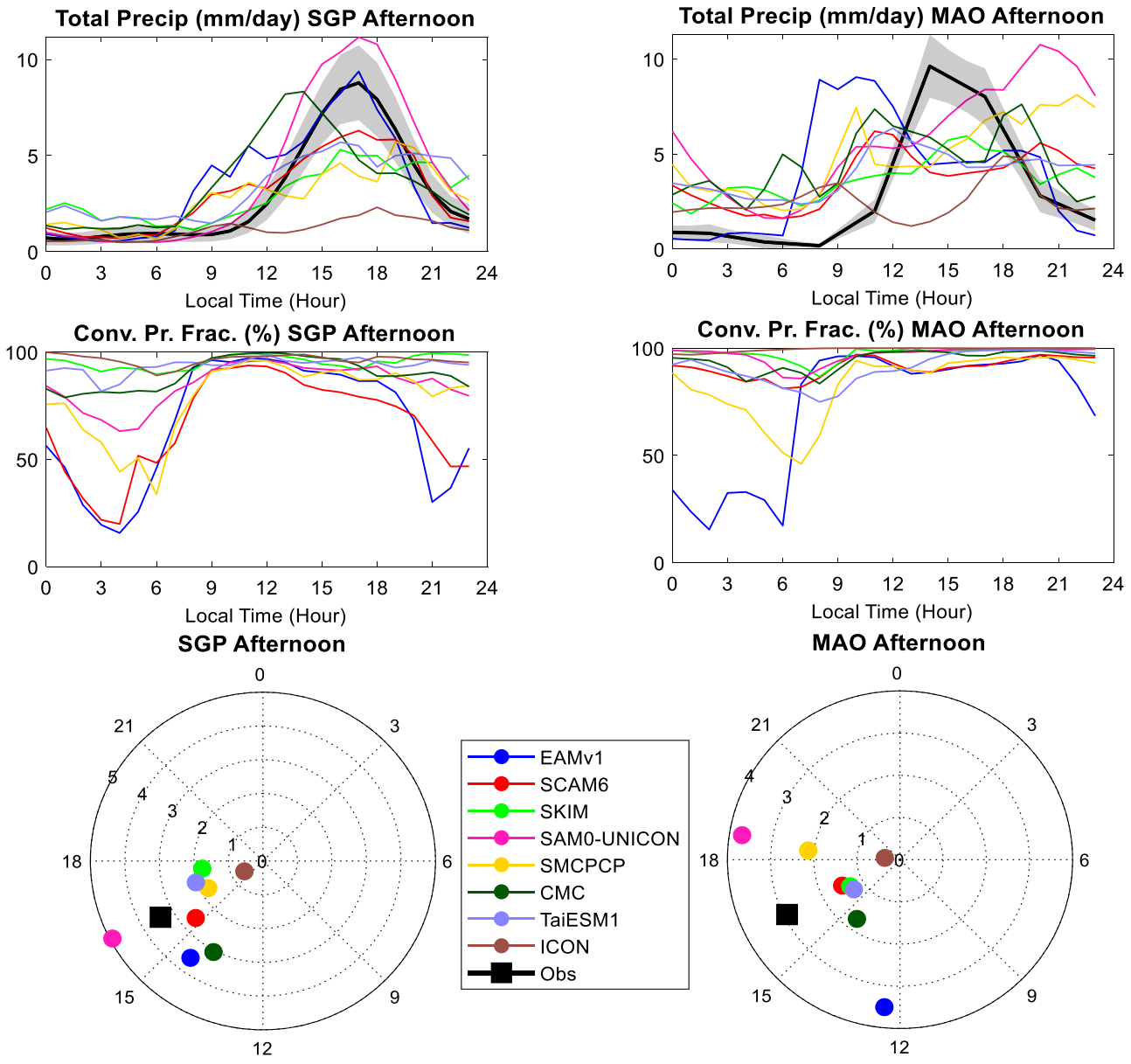

FIGURE 6 Diurnal cycle time series of (top) total precipitation rate (mm·day^{-1}), (middle) convective precipitation fraction, and (bottom) harmonic dial plots of total precipitation averaged for the selected afternoon precipitation days during the long-term simulation periods at (left) SGP and (right) MAO

convection case library visually selected from radar and satellite images (Tian *et al.*, 2021). The last criterion is set to exclude those cases of propagating MCSs with a daytime rainfall peak, which occur frequently during the rainy season at MAO and overlap with locally generated rainfall (Tang *et al.*, 2016). A nocturnal precipitation day at SGP and MAO is chosen when it has (a) peak rain rate greater than 1 mm·day^{-1}, and (b) rain peak time between 0000 and 0700 LST. Overall, there are 136 and 380 days selected for the afternoon and nocturnal precipitation days, respectively, during the 12 warm seasons at SGP, and 111 and 73 days selected for the afternoon and nocturnal precipitation days, respectively, during the 2 years at MAO.

3.2 | Afternoon precipitation regime

3.2.1 | Diurnal cycle of precipitation

The mean diurnal cycle of total precipitation and convective precipitation fraction for the selected afternoon precipitation days at SGP and MAO are shown in Figure 6. Also shown are the harmonic dial plots of total precipitation. The observations show that the afternoon regime precipitation picks up after 0900 LST at both sites, reaches a daily maximum around 1700 LST at SGP and 1400 LST at MAO, then decreases to late-night/early-morning values around 2100 LST. In the diurnal harmonic analysis,

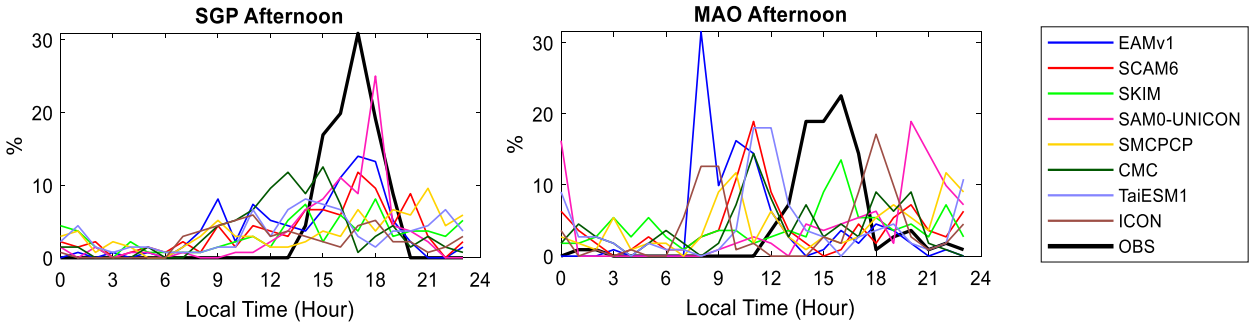

FIGURE 7 Percentage of days that the diurnal maximum precipitation occurs at each hour. The total number of cases are 136 days for SGP and 111 days for MAO

the diurnal phase of afternoon precipitation at SGP is well captured in most SCMs, as opposed to the time series of all events in Figure 2, while their diurnal amplitudes vary. At MAO, models have a large spread of afternoon precipitation peak time, consistent with the time series of all events in Figure 2. EAMv1 shows large precipitation in the morning with the diurnal phase peak at noon; SMCPCP and SAM0-UNICON have a late afternoon peak just after 1800 LST; SCAM6, SKIM and TaiESM1 capture the observed diurnal phase, but their diurnal amplitudes are much smaller. ICON produces two precipitation peaks, one in the morning and the other in the late afternoon, with much lower magnitude. The different model treatments of the preconditioning, triggering, developing of convection and convection interaction with environment via entrainment/detrainment may be responsible for the large spread or model performance. Another aspect is the presence of cold-pool environments and associated boundary-layer features and triggering of secondary developments, leading to the propagation as well as organization of convection (e.g. Oliveira *et al.*, 2020). It is also likely that these processes are complex and location-dependent, so that effort is needed to improve the current globally uniform convective parametrization.

Figure 7 shows the frequency of diurnal maximum precipitation occurrence at each hour. The model performance of maximum precipitation frequency is consistent with their performance of mean DCP in Figure 6. The maximum diurnal precipitation occurs mostly between 1500 and 1900 LST at SGP and 1300 and 1700 LST at MAO, consistent with the time of large mean diurnal precipitation (Figure 6). Models generally capture the maximum precipitation time at SGP, with a few percentages of time when models produce maximum precipitation too early or too late. At MAO, models frequently produce maximum precipitation either too early or too late compared to observation, except SKIM. This again indicates that the response of model precipitation to environment at moist tropical land is not as sophisticated as at midlatitude land.

3.2.2 | Apparent heating and drying

In the daytime, all models produce most of their precipitation from convection, with convective precipitation fraction close to 100% (second row of Figure 6). The model performance of afternoon convection is further examined by looking at the vertical profiles of apparent heating (Q_1) and drying (Q_2) in Figure 8. Q_1 and Q_2 were first introduced by Yanai *et al.* (1973) to estimate the diabatic processes:

$$Q_1 = \frac{1}{C_p}\left(\frac{\partial \bar{s}}{\partial t} + \bar{\vec{V}}\cdot\nabla\bar{s} + \bar{\omega}\frac{\partial \bar{s}}{\partial p}\right) = \frac{1}{C_p}\left(Q_{\mathrm{rad}} + L_v\left(d_{\mathrm{w}} + d_{\mathrm{i}}\right) - \frac{\partial \overline{\omega' s'}}{\partial p}\right), \quad (1)$$

$$Q_2 = -\frac{L_v}{C_p}\left(\frac{\partial \bar{q}}{\partial t} + \bar{\vec{V}}\cdot\nabla\bar{q} + \bar{\omega}\frac{\partial \bar{q}}{\partial p}\right) = \frac{L_v}{C_p}\left(d_{\mathrm{w}} + d_{\mathrm{i}} + \frac{\partial \overline{\omega' q'}}{\partial p}\right), \quad (2)$$

where $s = C_p T + gz$ is the dry static energy and C_p is the specific heat for dry air at constant pressure; q is water vapour mixing ratio; $\vec{V}$ is horizontal wind vector; ω is vertical velocity in pressure coordinate; Q_{rad} is radiative heating; $L_v\left(d_{\mathrm{w}} + d_{\mathrm{i}}\right)$ is the latent heat from liquid and ice processes; the overbar refers to a horizontal average and the prime refers to a deviation from the average. The "observed" Q_1 and Q_2 are derived from the large-scale dynamics (the centre part of the equations) from the variational analysis while the "simulated" Q_1 and Q_2 are the sum of all physical tendencies in the model (the right-hand side of the equations). The simulated vertical profiles of Q_1 and Q_2 are generally consistent with observations at SGP (Figure 8, left column), with heating peak in the middle to upper troposphere around 400 to 500 hPa. However, there are large discrepancies of Q_1 and Q_2 profiles at MAO (Figure 8, right column). Models produce a heating peak near 700 to 800 hPa, much lower than the observed

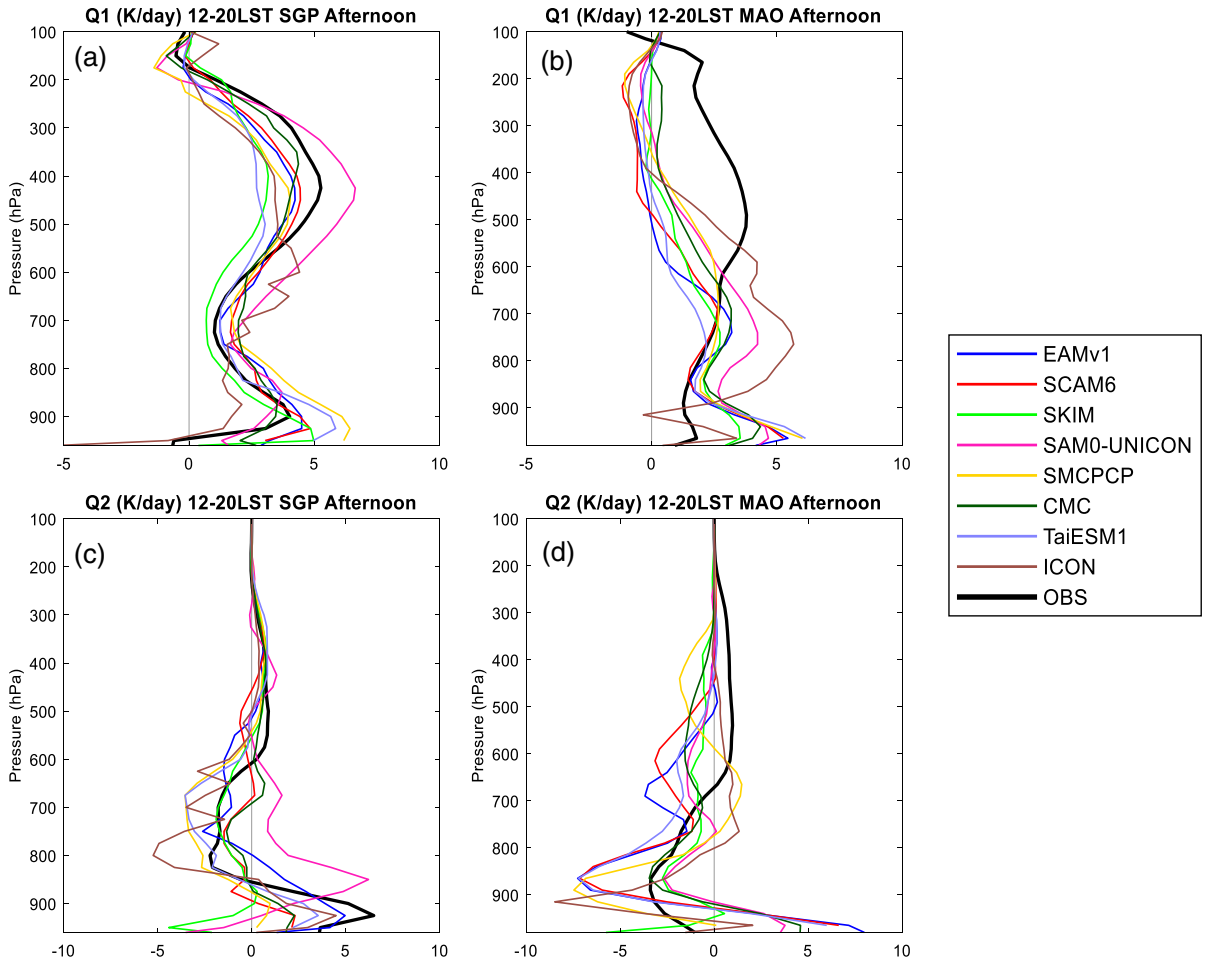

FIGURE 8 (a,b) Apparent heating (Q_1) and (c,d) drying (Q_2) (K·day^{-1}) averaged between 1200 and 2000 LST for selected afternoon precipitation days during the long-term simulation periods at (a,c) SGP and (b,d) MAO

peak at near 500 hPa. While the observed heating remains large to about 150 hPa, model heating is small about 500 hPa. They also fail to reproduce the observed moisture sink between 250 and 650 hPa. These discrepancies were also found in the Large-scale Biosphere–Atmosphere experiment (LBA) conducted in southwest Amazonia (Ma *et al.*, 2021a), indicating that models produce too shallow afternoon convection over the broad Amazon region. The fact that models simulate Q_1 and Q_2 well at SGP but poorly at MAO also highlights the dependence of model performances at different locations. The poor performance for deep convection at MAO despite being driven by observed large-scale forcing suggests significant common deficiencies in deep convective parametrization over tropical land.

3.2.3 | Deep convection triggering

At both SGP and MAO, a common model bias in DCP is the early onset of precipitation. The observed diurnal precipitation at both SGP and MAO picks up quickly near 1200 LST, while many models produce notable precipitation a few hours earlier (Figure 6). To further quantify the early onset of precipitation, we define the precipitation onset time as the first hour after 0600 LST when the precipitation at that hour increases above 1 mm·day^{-1}. The statistics of precipitation onset time are shown in Figure 9. The models we are discussing in this section are shown in thick lines, and those which will be discussed in Section 4 for sensitivity study are shown in thin lines. The mean onset time of precipitation is observed in early afternoon at SGP and around noon at MAO, about 3–4 hr earlier than the maximum precipitation time (Figure 7). However, the SCM-simulated onset time is usually 1 to 2 hr earlier than in observations at SGP, and up to 4 hr earlier at MAO, even for those models which produce maximum precipitation at a later time (Figure 7). CMC and ICON have a consistent mean precipitation onset time with observation at MAO, but their diurnal distribution is broader, with three (CMC) or two (ICON) precipitation peaks during the daytime (top-right panel of Figure 6).

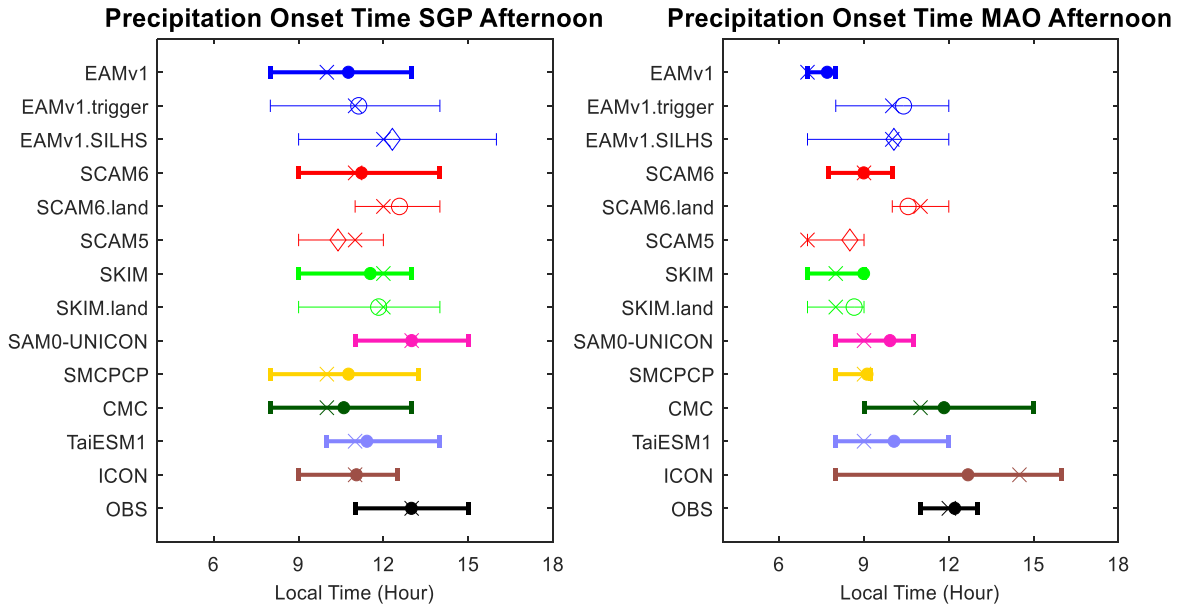

FIGURE 9 The mean (dot, circle or diamond), median (cross), 25th and 75th percentiles (vertical lines) of precipitation onset time for the afternoon precipitation days at (left) SGP and (right) MAO. Models for sensitivity studies in Section 4 are also shown here in thin lines

Among these SCMs, EAMv1, SCAM6, SMCPCP and ICON use convective available potential energy (CAPE) to trigger deep convection (Table 2). This CAPE-based convective trigger is believed to trigger convection too easily and too frequently (e.g. Xie and Zhang, 2000; Ma *et al.*, 2021b). A modified trigger using dynamic CAPE (dCAPE) introduced by Xie and Zhang (2000) and further enhanced in Xie *et al.* (2019) is implemented in EAMv1.trigger and shows promising results on mitigating the early onset of convection (see further discussion in Section 4). Using a convective inhibition (CIN)-based convective trigger, SKIM shows good precipitation onset time at SGP, but too early onset time at MAO, possibly due to the low-CIN environment in the Amazon permitting convection to trigger too easily but not through a sufficiently deep layer.

Another well-known issue of early onset of deep convection in GCMs is the poor simulation of the transition of shallow-to-deep convection and the gradual moistening of the free troposphere (Guichard *et al.*, 2004; Zhang and Klein, 2010). Shallow and deep convection are usually related to very different forcing regimes, entrainment and detrainment rates, and environment conditions. Therefore, almost all previous GCMs separate them into different schemes, and they work reasonably well in practice. However, separating the two schemes usually leads to an overly abrupt transition from one condition to another (e.g. Rio *et al.*, 2009). Deep convection is often triggered as soon as the large-scale environment reaches the triggering criterion in the model, instead of developing through an intermittent stage of preconditioning of the free atmosphere as in the real world. SAM0-UNICON uses a new parametrization that aims to unify shallow and deep convective schemes to simulate the complex interactions between subgrid and grid-scale processes such as the transition from shallow to deep convection. While it correctly simulates the precipitation onset time at SGP, at MAO in encounters a similar deficiency of ~2 hr earlier onset time (Figure 9). *It may be partly related to the inability of SCM to handle horizontal advection of subgrid cold pools*. This reveals a major challenge in unified parametrization to treat all conditions within a single set of equations and a need to test the models in global simulations.

3.3 | Nocturnal precipitation regime

3.3.1 | Diurnal cycle of precipitation

The mean diurnal cycle of total precipitation, convective precipitation fraction and the diurnal harmonic dial plots of total precipitation for nocturnal precipitation days are shown in Figure 10. Nocturnal precipitation is typically related to the elevated convection above a nocturnal stable boundary layer (e.g. Lee *et al.*, 2008; Geerts *et al.*, 2017) or propagating MCSs. The observations show a diurnal peak at ~0300 LST at SGP and ~0500 LST at MAO, with a diurnal peak of ~20 mm·day^{-1} and harmonic amplitude of ~8 mm·day^{-1}, much larger than the afternoon precipitation events in Figure 6. At 1200~1500 LST, precipitation at SGP reaches its diurnal minimum, while precipitation at MAO reaches a secondary peak, close to but weaker than

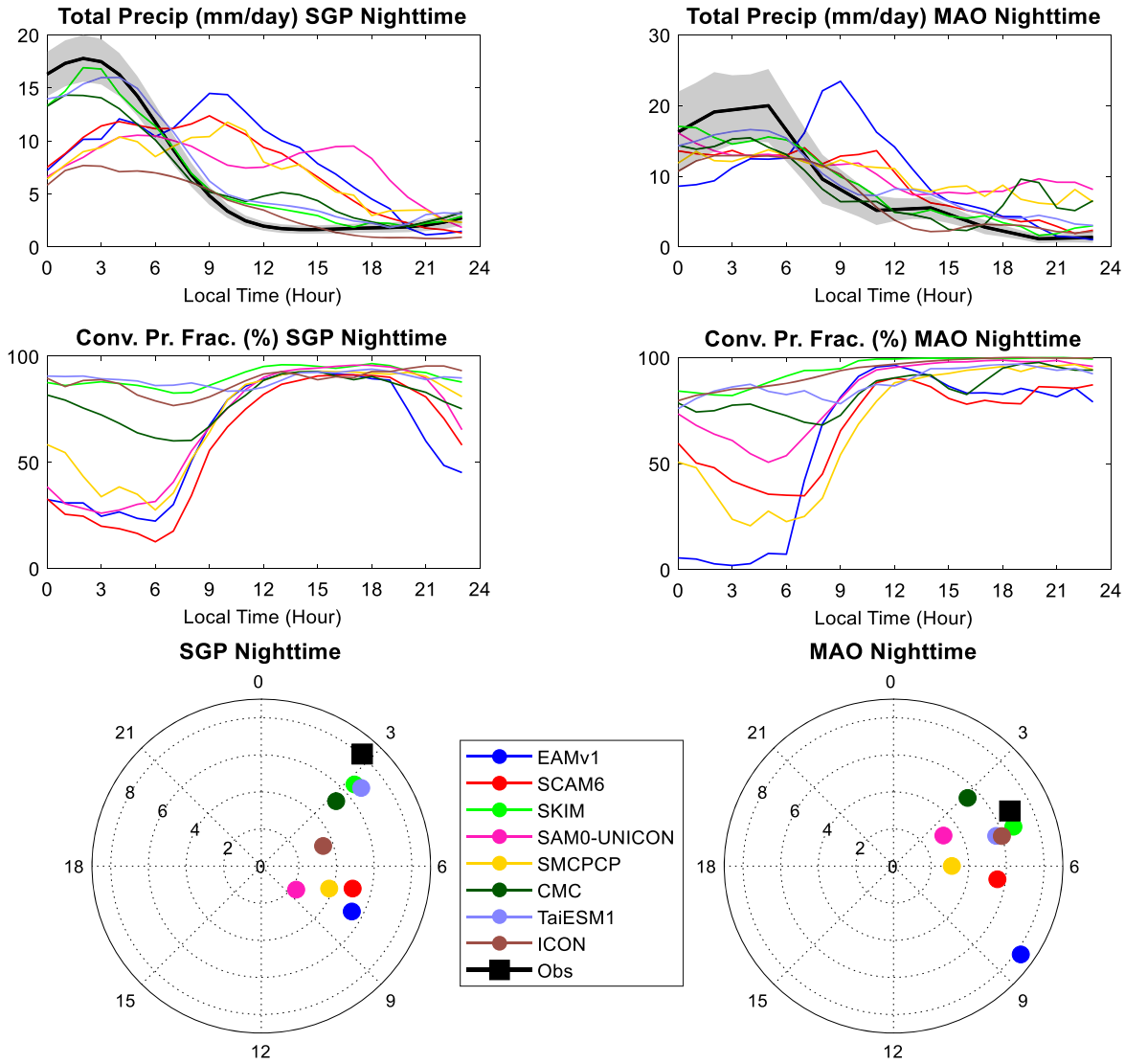

FIGURE 10 As in Figure 6 but for selected nocturnal precipitation days

the peak of afternoon precipitation. This indicates that even when the nocturnal precipitation has released some instability of the atmosphere, the solar heating in the following daytime and the moist environment can still trigger afternoon convection.

From Figure 10, SCMs can be divided into two groups in simulating nocturnal precipitation at SGP. SKIM, CMC and TaiESM1 well capture the diurnal phase and amplitude of nocturnal precipitation, and ICON also captures the diurnal phase but underestimates the amplitude of nocturnal precipitation. EAMv1, SCAM6, SAM0-UNICON and SMCPCP produce diurnal precipitation later with smaller magnitude. The models that well capture nocturnal precipitation at SGP also perform well at MAO, while the other models produce either a smaller magnitude or later phase of DCP. Between 0000 and 0600 LST, SKIM, CMC, TaiESM1 and ICON produce most of their precipitation (70%–90%) from the convective parametrization at both sites, while other models produce ~60% of their precipitation at SGP and 40%–95% of their precipitation at MAO as large-scale precipitation. Although impacted by convective process such as latent heating and detrainment, the large-scale precipitation produced in SCMs is primarily attributed to the prescribed large-scale forcing, which is constrained by the observed surface precipitation. In free-run GCMs, where the large-scale forcing *interacts with model physics and is affected by their deficiencies*, the simulation of nocturnal precipitation could be even worse (e.g. Tang *et al.*, 2021). Thus, it seems to be necessary to improve the deficiencies in model parametrizations found in the present study that might potentially contribute to model errors in a less constrained model set-up.

There is a distinguishing feature that separates these two groups of models: whether or not the model allows

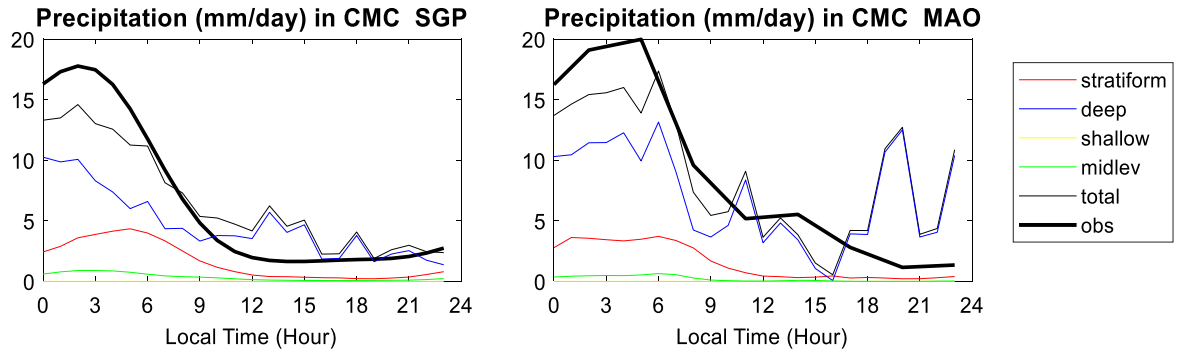

FIGURE 11 Precipitation rates (mm·day^{-1}) from different components in CMC model for selected nocturnal precipitation days at (left) SGP and (right) MAO

elevated convection triggered above the boundary layer. EAMv1, SCAM6 and SMCPCP all use the ZM deep convective scheme with the launching parcel chosen only within the boundary layer. SKIM and TaiESM1 select air parcels below ~700 hPa ($\sigma = 0.7$) and 600 hPa, respectively, and ICON selects air parcels within 350 hPa above the surface. It is natural to hypothesize that allowing convection to occur above the boundary layer is the key to simulating nocturnal convection. In the sensitivity study in Section 4, when the default ZM scheme is modified by unlimiting the launching level, the nocturnal precipitation in EAMv1.trigger is significantly improved compared to default EAMv1. CMC has a separated mid-level convective scheme to capture elevated convection (McTaggart-Cowan *et al.*, 2020). The mid-level scheme exhibits a maximum activity during the night (Figure 11). However, its contribution to the total precipitation is very modest while deep convection contributes the most for nocturnal precipitation. Further sensitivity tests with different thresholds for deep and mid-level convection triggering have shown little sensitivity of the phase of DCP to how active the deep and mid-level schemes are.

3.3.2 | Apparent heating and drying

Figure 12 shows the 0000–0600 LST mean vertical profiles of Q_1 and Q_2 at SGP and MAO for the nocturnal precipitation events. The observed heating profile is top-heavy at SGP and roughly parabolic at MAO, showing typical convective conditions over midlatitude continent and tropics, respectively. The condensational drying has a sharper and stronger peak at MAO than SGP. It is interesting to see that all models produce heating and drying peaks at a similar height to that of the observed, despite their wide ranges of convective fraction as shown in Figures 6 and 10 (e.g. Schumacher *et al.*, 2004). The reasonable simulation of nocturnal convective heating depth at MAO (Figure 12b) is notable given the poor performance at afternoon convective heating depth (Figure 8b), possibly related to the fact that afternoon convection is locally driven while nocturnal convection is propagating organized convection. The magnitude of Q_1 and Q_2 varies among models. SKIM, TaiESM1 and CMC produce similar magnitudes of Q_1 and Q_2 comparable with observations, while the other models produce smaller magnitudes (except ICON Q_1 at MAO). The reduction of the Q_1 peak in these models is more prevalent in the upper levels, which may be related to the weaker convective activity that is not sufficient to remove all the instability from the large-scale forcing. The remaining instability in these models is then released at a later time, causing the morning-time precipitation peak seen in Figure 10.

4 | SENSITIVITY STUDY

In addition to the default simulations, some modelling centres also performed other simulations using different model versions, physical schemes or configurations. Table 3 shows the information of the simulations included in this section emphasizing their differences from the default models/runs. DCP in SKIM.nudge is very similar to the default runs, so we choose not to show them to make the figures more readable. Moreover, SAM0-UNICON is included in this sensitivity study for two reasons: firstly, it is developed from SCAM5, with the same turbulence, microphysics and macrophysics schemes but a different convective scheme; secondly, it unifies shallow and deep convection, so we feel it is interesting to compare it with another model with unified shallow and deep convection (EAMv1.SILHS).

Figure 13 shows DCP performance of the models for sensitivity study in the afternoon precipitation regime, while Figure 14 shows DCP performance in the nocturnal precipitation regime. EAMv1.trigger uses a modified convective trigger, which uses a dynamic CAPE (dCAPE:

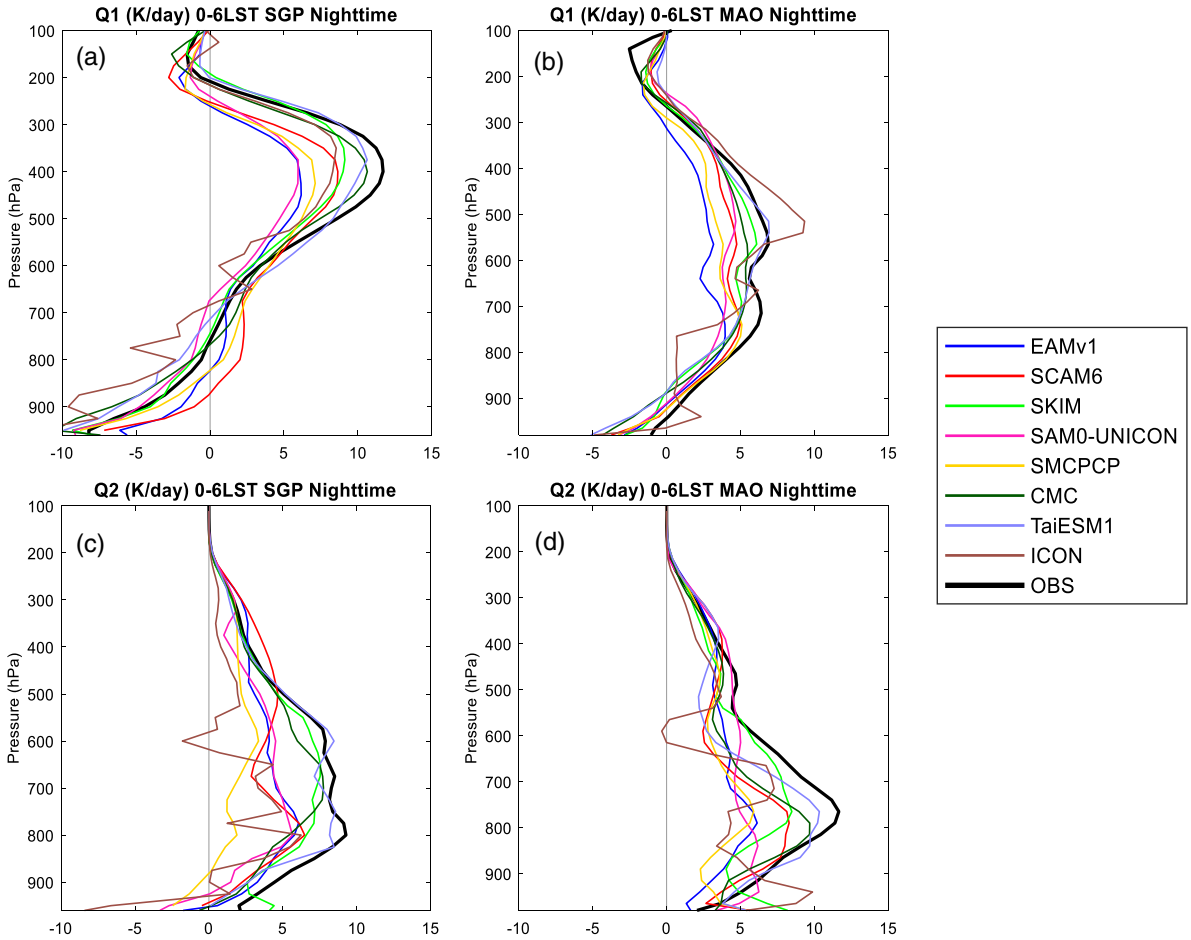

FIGURE 12 (a,b) Q_1 and (c,d) Q_2 (K·day^{-1}) averaged between 0000 and 0600 LST for selected nocturnal precipitation days at (a,c) SGP and (b,d) MAO

TABLE 3 Model information for sensitivity study

Model name	Model features	References
EAMv1	Deep convection: ZM with convective trigger: (1) CAPE >70 J·kg^{-1} (2) The air parcel launch level is chosen within the boundary layer	
EAMv1.Trigger	Deep convection: ZM with convective trigger: (1) CAPE >0 (2) dCAPE >0 (3) The air parcel launch level is chosen between the surface and 600 hPa	Xie *et al.* (2019)
EAMv1.SILHS	Deep convection: CLUBB-SILHS	Thayer-Calder *et al.* (2015); Larson (2017)
SAM0-UNICON	Turbulence: diag_TKE Stratiform clouds: MG, Park1 Shallow convection: UNICON Deep convection: UNICON	Park *et al.* (2019)
SCAM6	Turbulence: CLUBB Stratiform clouds: MG2, CLUBB Shallow convection: CLUBB Deep convection: ZM	Gettelman *et al.* (2019)
SCAM5	Turbulence: diag_TKE Stratiform clouds: MG, Park1 Shallow convection: PB09 Deep convection: ZM	Neale *et al.* (2012)
SCAM6.land	Interactive land	
SKIM.land	Interactive land	
SKIM.nudge	Nudging temperature and moisture	

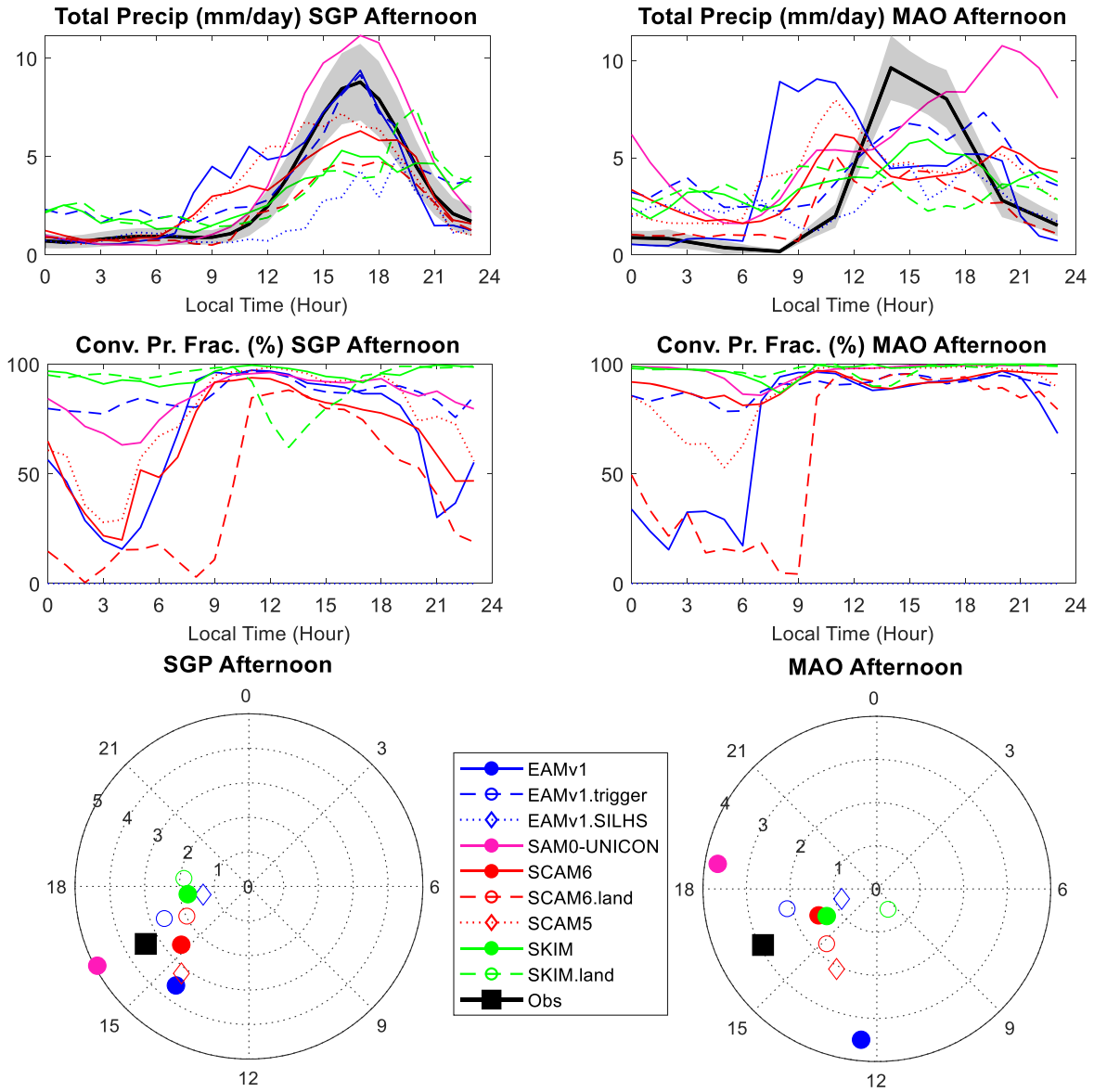

FIGURE 13 As in Figure 6 but for selected models/configurations for sensitivity study. Sensitivity runs are indicated by dashed/dotted lines and open symbols. Note that the convective precipitation fraction for EAMv1.SILHS (blue dotted line) is zero because the convective and large-scale precipitation is unified in CLUBB-SILHS

CAPE changes due to large-scale advections) to trigger convection and allow air parcels to launch above the boundary layer. The improvement of DCP in GCMs has been demonstrated in Xie *et al.* (2019), Wang *et al.* (2020) and Cui *et al.* (2021). Here for SCM, the improvement of DCP is also shown at SGP and MAO (Figures 13 and 14) (blue dashed line and open circle). We believe that the dCAPE trigger helps delay the precipitation onset of afternoon precipitation, while allowing air parcels to launch above the boundary layer helps convection occur at night.

Another independent modification of EAMv1, EAMv1.SILHS, also shows significant improvement on DCP in the two precipitation regimes. Instead of using ZM for deep convection and CLUBB for shallow convection and large-scale clouds and precipitation in the default EAMv1, EAMv1.SILHS uses CLUBB for all shallow convection, deep convection and large-scale clouds and precipitation. Therefore, the convective fraction is zero because it does not separate convective and large-scale precipitation. The CLUBB is interfaced to the microphysics scheme using the subgrid sampler SILHS. It well captures the elevated convection at night as shown in Figure 14, possibly because it does not need a convective trigger nor specification of parcel launching level. For afternoon precipitation, it delays the precipitation onset time at both SGP and MAO (Figure 9), but only produces about half of the observed peak precipitation and ~30%

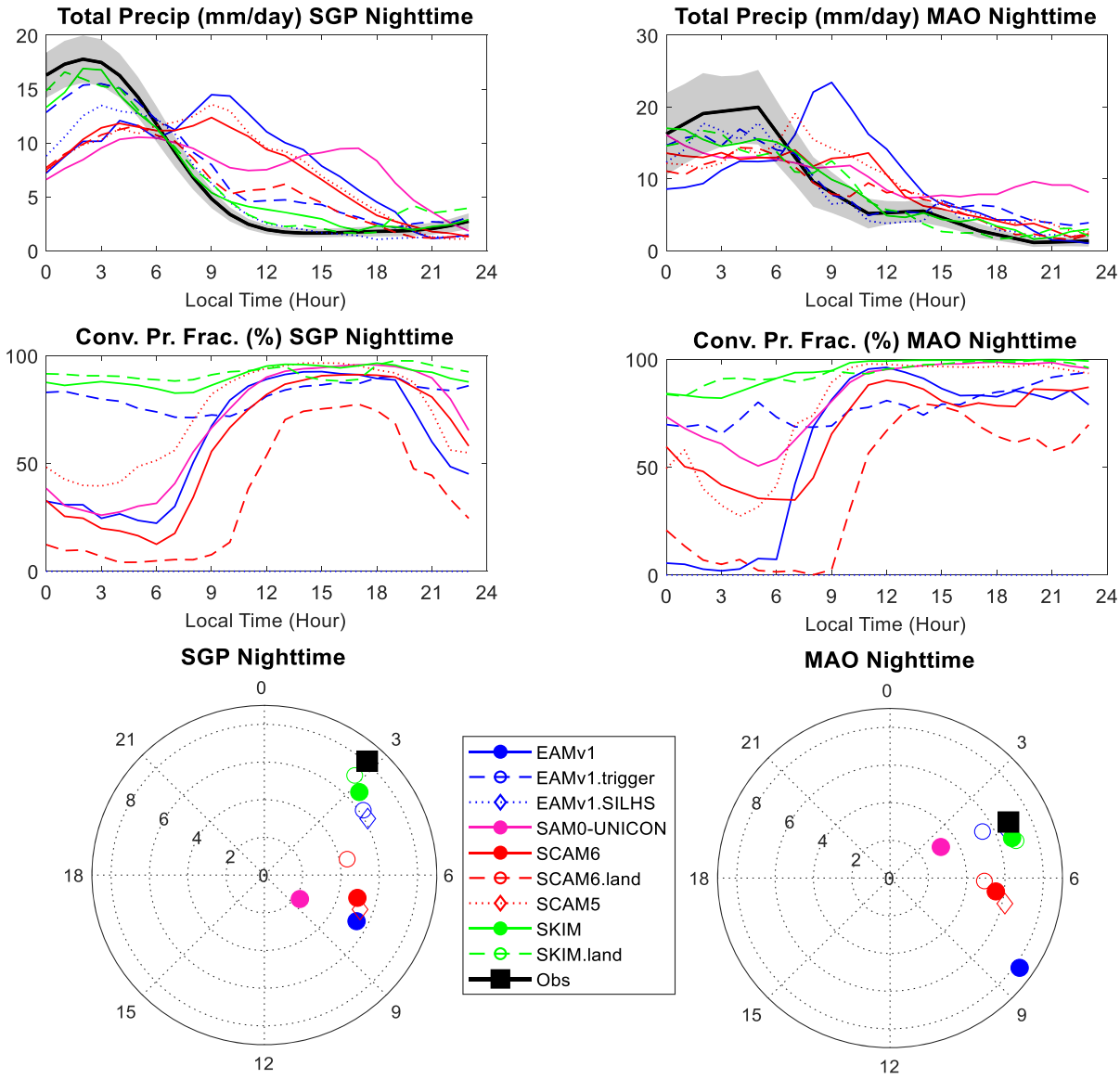

FIGURE 14 As in Figure 13 but for nocturnal precipitation days

of the harmonic amplitude (Figure 13). This is subject to further improvements.

Another model with a unified convective scheme, SAM0-UNICON, is also shown in Figures 13 and 14. Note that SAM0-UNICON and SCAM6 both have a tight relationship with SCAM5; SAM0-UNICON has the same turbulence, microphysics and macrophysics schemes as SCAM5, but a different shallow and deep convective scheme. SCAM6 only shares the same deep convective scheme with SCAM5, with turbulence, shallow convection and macrophysics replaced by CLUBB. The DCP performance in SCAM6 is similar to that in SCAM5, while SAM0-UNICON shows larger differences with SCAM5. This indicates that DCP is primarily controlled by the deep convective scheme. Since SAM0-UNICON can simulate the complex interactions between subgrid and grid-scale processes such as the transition from shallow to deep convection, it captures well the afternoon precipitation, especially at SGP. However, its performance on night-time precipitation still needs to be improved. This is consistent with previous work in global simulations (Park, 2014b; Tang *et al.*, 2021).

Two models conducted sensitivity tests with an interactive land model. SCAM6 is coupled with the Community Land Model version 5.0 (CLM5: Lawrence *et al.*, 2019), while SKIM is coupled with the revised Noah land surface model version 3.4.1 (Koo *et al.*, 2017). SKIM.land performs similar to the default SKIM run, while SCAM6.land performs better than SCAM6, with the early onset of afternoon precipitation (Figures 9 and 13) and the morning rainfall in nocturnal precipitation days (Figure 14) both reduced. It is interesting to see that SCAM6.land produces

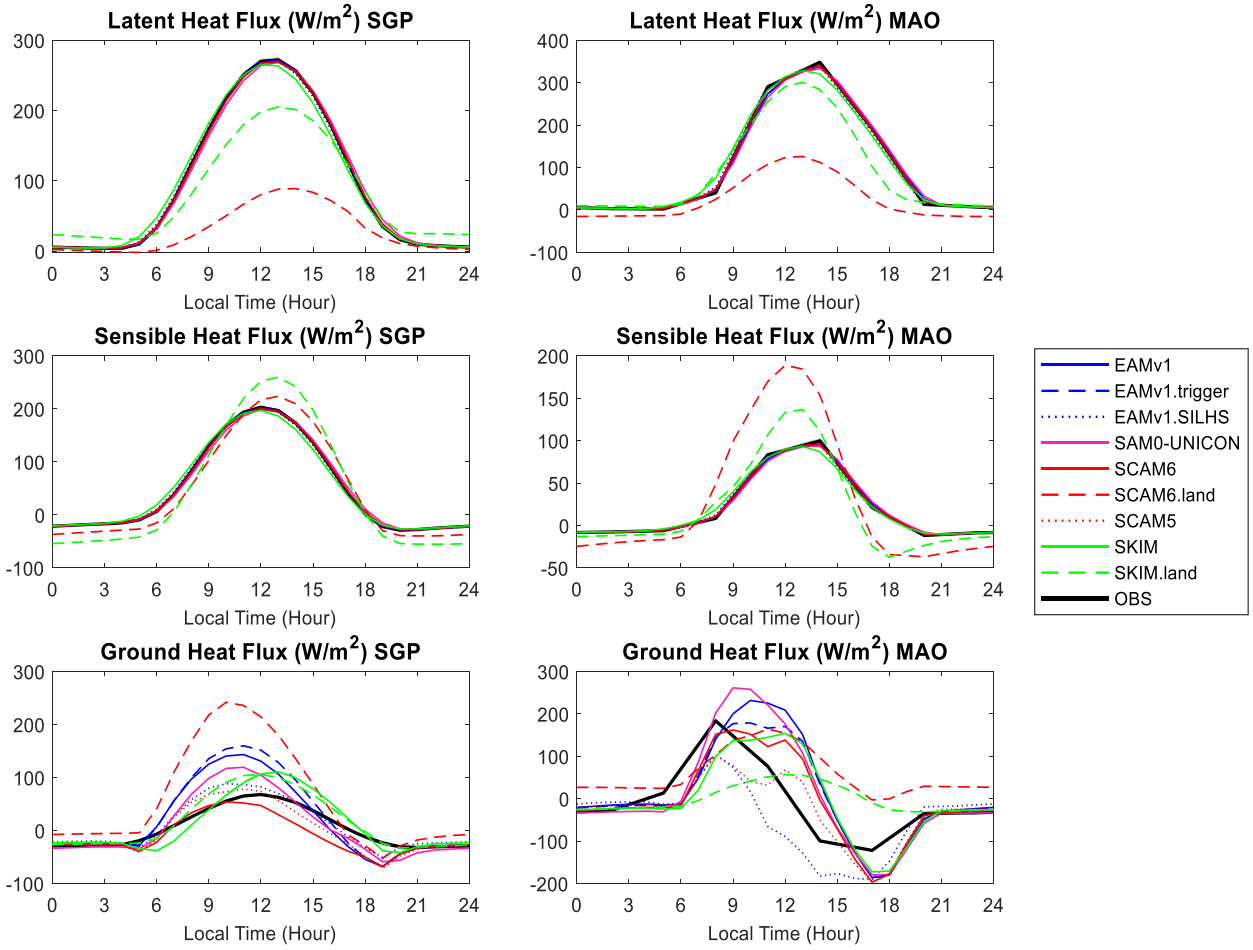

FIGURE 15 The diurnal cycle of (top) surface latent heat, (middle) sensible heat fluxes and (bottom) ground heat flux (net radiative fluxes minus latent and sensible heat fluxes) ($W \cdot m^{-2}$) averaged for the long-term simulation periods at (left) SGP and (right) MAO. The diurnal cycle averaged in afternoon and nocturnal precipitation days have similar performance (not shown)

much lower latent heat fluxes and higher sensible heat fluxes than observations (Figure 15). The estimated ground heat flux is also much larger in SCAM6.land than in other models, with daily mean of 61.7 $W \cdot m^{-2}$ at SGP and 59.0 $W \cdot m^{-2}$ at MAO. The corresponding ground heat flux in SCAM6 is –9.4 $W \cdot m^{-2}$ at SGP and –3.9 $W \cdot m^{-2}$ at MAO, and that in the observations is 4.9 $W \cdot m^{-2}$ at SGP and –5.3 $W \cdot m^{-2}$ at MAO. On the other hand, SKIM.land also produces lower latent heat fluxes and higher sensible heat fluxes than observations, likely due to more humid near-surface air or misrepresented surface conditions such as vegetation fraction, land type or soil properties. Its turbulent flux errors are smaller than SCAM6.land, and its ground heat flux is similar with SKIM and observations. Despite the differences in the land models used in SCAM6.land and SKIM.land, it may be inferred that the land–atmospheric interactions in climate models are not well represented so that a model (SCAM6.land) needs to produce more unrealistic surface fluxes in order to get more realistic precipitation in deep convective regimes.

5 | SUMMARY AND DISCUSSIONS

The diurnal cycle of precipitation (DCP) is a problem that GCMs have struggled to represent in past decades (Fiedler *et al.*, 2020). Although the latest GCMs in the recent CMIP6 have shown improvement in simulating DCP (Tang *et al.*, 2021), they still suffer from the persistent problems of too early precipitation and missing nocturnal precipitation.

The GEWEX Global Atmospheric System Study (GASS) panel organized a project focusing on understanding and improving the model capability to simulate diurnal precipitation phenomena through multi-model intercomparison studies against observations. This study focuses on the intercomparison of SCMs to understand what processes control the diurnal cycle of precipitation over different climate regimes and identify the deficiencies and missing physics in current model parametrizations. Instead of focusing on a particular intensive observing period for several days to a few months as in previous SCM

intercomparison studies, we have performed long-term hindcast simulations to obtain robust statistics of model performances on DCP. Eleven SCMs from different modelling centres around the world have participated in this project.

DCP in 12 summer seasons at a midlatitude land site (SGP) and two continuous years at a tropical land site (MAO) are investigated in this study. The two selected sites have distinguished and representative characteristics of the large-scale environment, clouds and precipitation. The participating SCMs do not always show the same discrepancies at the two sites. This indicates that some parametrization assumptions may not work well across all climate regimes.

Two regimes of DCP are examined in this study; one is surface-driven afternoon convection and the other is nocturnal precipitation caused by elevated convection or propagating convective systems. For afternoon convection, precipitation in most SCMs initiated 1 to 4 hr earlier than observation. The early onset of precipitation is more severe at MAO than at SGP. It appears to be associated with two other issues common across all the models for MAO afternoon precipitation cases: a severe deficiency of convective heating in the upper troposphere, and rainfall too evenly spread across times of day. In other words, for the MAO afternoon cases, models fail to develop strong deep convection but precipitate too easily from convection in the lower troposphere. At SGP, the early onset of afternoon precipitation may be due to the missing transition of shallow-to-deep convection in climate models. More sophisticated parametrizations that unify shallow and deep convection (e.g. UNICON, CLUBB-SILHS) can improve the early onset problem, although UNICON shows more deficiencies in the precipitation–CRH relationship. For nocturnal precipitation, although all SCMs produce considerable precipitation at night, the partitioning of convective precipitation and large-scale precipitation differs dramatically among models. Models with most of the nocturnal precipitation generated from large-scale are likely driven by the prescribed large-scale forcing. SCMs that produce most of nocturnal precipitation from convection (SKIM, TaiESM1, CMC, ICON and EAMv1.trigger) all allow convection to be triggered above the boundary layer. Although a few recent studies have considered convection moving across grids (Malardel and Bechtold, 2019; McTaggart-Cowan *et al.*, 2019b), most SCMs and their parent GCMs still struggle to propagate convection from one grid to another. The capability to detect mid-level instability above the boundary layer is important for them to simulate nocturnal precipitation.

Sensitivity studies were performed using continuous nudging runs, different parametrizations, or interactive land models. Using a revised convective trigger specifically targeting improvement on the diurnal cycle of precipitation, EAMv1.trigger shows the importance of dynamically constraining the convective trigger and allowing parcels to launch above the boundary layer in traditional convective parametrizations to produce precipitation at the right time. The representation of the shallow convection phase and its transition to deep convection is still a key aspect to be improved in models. One path towards improving this feature is the effort of unifying shallow and deep convection, as seen in SAM0-UNICON and EAMv1.SILHS. On the other hand, in the two land–atmosphere coupled simulations, the one with larger biases in surface turbulent fluxes (SCAM6.land) shows more improvement on DCP. This indicates that the relationship between the land–atmospheric interaction and DCP is complicated and points to the importance of the representation of boundary-layer processes in deep convective regimes. Further study is needed to investigate how the representation of land–atmospheric coupling will influence simulation of DCP.

Although not the focus of this study here, the discrepancy in the amplitude of DCP should also be pointed out. In addition to deep and shallow convection, boundary-layer processes can highly contribute to the control of the diurnal amplitude (e.g. Koo and Hong, 2010). Therefore, a diversity of turbulence schemes (Table 1) might be a source of large spread in diurnal amplitude, which needs to be addressed in future study.

This SCM intercomparison study provides insights of which physical processes are essential in climate models to simulate DCP, given a large-scale environment close to the real world. In a global or regional model, the model biases in large-scale dynamic and thermodynamic states and the interactions between the large-scale fields and physics also impact the simulation of DCP. This is not revealed in the SCM study. An intercomparison of global and regional climate models is currently underway and more details will be presented on DCP over broader regions in the near future.

ACKNOWLEDGEMENTS

This work is part of the GEWEX Global Atmospheric System Study (GASS) panel's Diurnal Cycle of Precipitation project. Work at LLNL is supported by the Earth and Environmental System Modeling, Regional and Global Model Analysis, Atmospheric System Research and Atmospheric Radiation Measurement programmes, funded by the US Department of Energy, Office of Science, Office of Biological and Environmental Research, and performed under the auspices of the US DOE by Lawrence Livermore National Laboratory under Contract DE-AC52-07NA27344. S. Tang was partially supported by the "Enabling Aerosol–cloud interactions at GLobal

convection-permitting scalES (EAGLES)" project (74358) funded by the US Department of Energy, Office of Science, Office of Biological and Environmental Research, Earth System Model Development programme. Pacific Northwest National Laboratory (PNNL) is operated for DOE by Battelle under contract DE-AC05-76RL01830. J.D. Neelin was supported by NSF project AGS-1936810.

AUTHOR CONTRIBUTIONS

Shuaiqi Tang: Conceptualization; formal analysis; investigation; methodology; resources; validation; visualization; writing – original draft. **Shaocheng Xie:** Conceptualization; investigation; methodology; supervision; writing – review and editing. **Zhun Guo:** Resources; writing – review and editing. **Songyou Hong:** Resources; writing – review and editing. **Boualem Khouider:** Resources; writing – review and editing. **Daniel Klocke:** Resources; writing – review and editing. **Martin Köhler:** Resources; writing – review and editing. **Myung-Seo Koo:** Resources; writing – review and editing. **R Phani:** Resources; writing – review and editing. **Vincent Larson:** Resources; writing – review and editing. **Sungsu Park:** Resources; writing – review and editing. **Paul A Vaillancourt:** Resources; writing – review and editing. **Yi-Chi Wang:** Resources; writing – review and editing. **Jing Yang:** Resources; writing – review and editing. **Chimene Daleu:** Resources; writing – review and editing. **Cameron R Homeyer:** Resources; writing – review and editing. **Todd R Jones:** Resources; writing – review and editing. **Neelam Malap:** Resources; writing – review and editing. **Roel A. J. Neggers:** Resources; writing – review and editing. **Thara V Prabha:** Resources; writing – review and editing. **Enver Ramirez:** Resources; writing – review and editing. **Courtney Schumacher:** Resources; writing – review and editing. **Cheng Tao:** Data curation; investigation; writing – review and editing. **Peter Bechtold:** Conceptualization; writing – review and editing. **Hsi-Yen Ma:** Conceptualization; data curation; writing – review and editing. **David Neelin:** Conceptualization; writing – review and editing. **Xubin Zeng:** Conceptualization; writing – review and editing.

ORCID

Shuaiqi Tang https://orcid.org/0000-0002-8946-9205
Shaocheng Xie https://orcid.org/0000-0001-8931-5145
Myung-Seo Koo https://orcid.org/0000-0002-6692-8181
Peter Bechtold https://orcid.org/0000-0002-1967-3382

REFERENCES

Bae, S.Y., Hong, S.-Y. and Lim, K.-S.S. (2016) Coupling WRF double-moment 6-class microphysics schemes to RRTMG radiation scheme in Weather Research Forecasting model. *Advances in Meteorology*, 2016, 5070154. https://doi.org/10.1155/2016/5070154.

Bašták Ďurán, I., Kohler, M., Eichhorn-Müller, A., Maurer, V., Schmidli, J., Schomburg, A., Klocke, D., Göcke, T., Schäfer, S., Schlemmer, L. and Dewani, N. (2021) The ICON single-column mode. *Atmosphere*, 12, 906. https://doi.org/10.3390/atmos12070906.

Bechtold, P., Redelsperger, J.-L., Beau, I., Blackburn, M., Brinkop, S., Grandper, J.-Y., Grant, A., Gregory, D., Guichard, F., How, C. and Ioannidou, E. (2000) A GCSS model intercomparison for a tropical squall line observed during TOGA-COARE. II: Intercomparison of single-column models and a cloud-resolving model. *Quarterly Journal of the Royal Meteorological Society*, 126(564), 865–888. https://doi.org/10.1002/qj.49712656405.

Bechtold, P., Bazile, E., Guichard, F., Mascart, P. and Richard, E. (2001) A mass-flux convection scheme for regional and global models. *Quarterly Journal of the Royal Meteorological Society*, 127(573), 869–886. https://doi.org/10.1002/qj.49712757309.

Bechtold, P., Chaboureau, J.-P., Beljaars, A., Betts, A.K., Köhler, M., Miller, M. and Redelsperger, J.-L. (2004) The simulation of the diurnal cycle of convective precipitation over land in a global model. *Quarterly Journal of the Royal Meteorological Society*, 130(604), 3119–3137. https://doi.org/10.1256/qj.03.103.

Bechtold, P., Köhler, M., Jung, T., Doblas-Reyes, F., Leutbecher, M., Rodwell, M.J., Vitart, F. and Balsamo, G. (2008) Advances in simulating atmospheric variability with the ECMWF model: from synoptic to decadal time-scales. *Quarterly Journal of the Royal Meteorological Society*, 134(634), 1337–1351. https://doi.org/10.1002/qj.289.

Bechtold, P., Semane, N., Lopez, P., Chaboureau, J.-P., Beljaars, A. and Bormann, N. (2014) Representing equilibrium and nonequilibrium convection in large-scale models. *Journal of the Atmospheric Sciences*, 71, 734–753. https://doi.org/10.1175/jas-d-13-0163.1.

Betts, A.K. and Jakob, C. (2002) Study of diurnal cycle of convective precipitation over Amazonia using a single column model. *Journal of Geophysical Research*, 107(D23), 4732. https://doi.org/10.1029/2002jd002264.

Bogenschutz, P.A., Tang, S., Caldwell, P.M., Xie, S., Lin, W. and Chen, Y.S. (2020) The E3SM version 1 single-column model. *Geoscientific Model Development*, 13, 4443–4458. https://doi.org/10.5194/gmd-13-4443-2020.

Bretherton, C.S., Krueger, S.K., Wyant, M.C., Bechtold, P., Van Meijgaard, E., Stevens, B. and Teixeira, J. (1999) A GCSS boundary-layer cloud model intercomparison study of the first ASTEX Lagrangian experiment. *Boundary-Layer Meteorology*, 93, 341–380. https://doi.org/10.1023/A:1002005429969.

Bretherton, C.S., Peters, M.E. and Back, L.E. (2004) Relationships between water vapor path and precipitation over the tropical oceans. *Journal of Climate*, 17, 1517–1528. https://doi.org/10.1175/1520-0442(2004)017<1517:Rbwvpa>2.0.Co;2.

Bretherton, C.S. and Park, S. (2009) A new moist turbulence parameterization in the community atmosphere model. *Journal of Climate*, 22, 3422–3448. https://doi.org/10.1175/2008JCLI2556.1.

Covey, C., Gleckler, P.J., Doutriaux, C., Williams, D.N., Dai, A., Fasullo, J., Trenberth, K. and Berg, A. (2016) Metrics for the diurnal cycle of precipitation: toward routine benchmarks for climate models. *Journal of Climate*, 29, 4461–4471. https://doi.org/10.1175/jcli-d-15-0664.1.

Cui, Z., Zhang, G.J., Wang, Y. and Xie, S. (2021) Understanding the roles of convective trigger functions in the diurnal cycle of precipitation in the NCAR CAM5. *Journal of Climate*, 34, 6473–6489. https://doi.org/10.1175/jcli-d-20-0699.1.

Dai, A., Trenberth, K.E. and Karl, T.R. (1999) Effects of clouds, soil moisture, precipitation, and water vapor on diurnal temperature range. *Journal of Climate*, 12, 2451–2473. https://doi.org/10.1175/1520-0442(1999)012<2451:Eocsmp>2.0.Co;2.

Dai, A. (2006) Precipitation characteristics in eighteen coupled climate models. *Journal of Climate*, 19, 4605–4630. https://doi.org/10.1175/jcli3884.1.

Davies, L., Jakob, C., Cheung, K., Del Genio, A., Hill, A., Hume, T., Keane, R.J., Komori, T., Larson, V.E., Lin, Y., Liu, X., Nielsen, B.J., Petch, J., Plant, R.S., Singh, M.S., Shi, X., Song, X., Wang, W., Whitall, M.A., Wolf, A., Xie, S. and Zhang, G. (2013) A single-column model ensemble approach applied to the TWP-ICE experiment. *Journal of Geophysical Research – Atmospheres*, 118, 6544–6563. https://doi.org/10.1002/jgrd.50450.

de Rooy, W.C., Bechtold, P., Fröhlich, K., Hohenegger, C., Jonker, H., Mironov, D., Siebesma, A.P., Teixeira, J. and Yano, J.-I. (2013) Entrainment and detrainment in cumulus convection: an overview. *Quarterly Journal of the Royal Meteorological Society*, 139(670), 1–19. https://doi.org/10.1002/qj.1959.

Del Genio, A.D. (2012) Representing the sensitivity of convective cloud systems to tropospheric humidity in general circulation models. *Surveys in Geophysics*, 33, 637–656. https://doi.org/10.1007/s10712-011-9148-9.

Del Genio, A.D., Chen, Y., Kim, D. and Yao, M.-S. (2012) The MJO transition from shallow to deep convection in CloudSat/-CALIPSO data and GISS GCM simulations. *Journal of Climate*, 25, 3755–3770. https://doi.org/10.1175/jcli-d-11-00384.1.

Eyring, V., Bony, S., Meehl, G.A., Senior, C.A., Stevens, B., Stouffer, R.J. and Taylor, K.E. (2016) Overview of the coupled model intercomparison project phase 6 (CMIP6) experimental design and organization. *Geoscientific Model Development*, 9, 1937–1958. https://doi.org/10.5194/gmd-9-1937-2016.

Fiedler, S., Crueger, T., D'Agostino, R., Peters, K., Becker, T., Leutwyler, D., Paccini, L., Burdanowitz, J., Buehler, S.A., Cortes, A.U., Dauhut, T., Dommenget, D., Fraedrich, K., Jungandreas, L., Maher, N., Naumann, A.K., Rugenstein, M., Sakradzija, M., Schmidt, H., Sielmann, F., Stephan, C., Timmreck, C., Zhu, X.H. and Stevens, B. (2020) Simulated tropical precipitation assessed across three major phases of the Coupled Model Intercomparison Project (CMIP). *Monthly Weather Review*, 148, 3653–3680. https://doi.org/10.1175/mwr-d-19-0404.1.

Frenkel, Y., Khouider, B. and Majda, A.J. (2011a) Simple multicloud models for the diurnal cycle of tropical precipitation. Part I: Formulation and the case of the tropical oceans. *Journal of the Atmospheric Sciences*, 68, 2169–2190. https://doi.org/10.1175/2011jas3568.1.

Frenkel, Y., Khouider, B. and Majda, A.J. (2011b) Simple multicloud models for the diurnal cycle of tropical precipitation. Part II: The continental regime. *Journal of the Atmospheric Sciences*, 68, 2192–2207. https://doi.org/10.1175/2011jas3600.1.

Geerts, B., Parsons, D., Ziegler, C.L., Weckwerth, T.M., Biggerstaff, M.I., Clark, R.D., Coniglio, M.C., Demoz, B.B., Ferrare, R.A., Gallus, W.A., Jr., Haghi, K., Hanesiak, J.M., Klein, P.M., Knupp, K.R., Kosiba, K., McFarquhar, G.M., Moore, J.A., Nehrir, A.R., Parker, M.D., Pinto, J.O., Rauber, R.M., Schumacher, R.S., Turner, D.D., Wang, Q., Wang, X.G., Wang, Z. and Wurman, J. (2017) The 2015 Plains elevated convection at night field project. *Bulletin of the American Meteorological Society*, 98, 767–786. https://doi.org/10.1175/bams-d-15-00257.1.

Gettelman, A., Morrison, H., Santos, S., Bogenschutz, P. and Caldwell, P.M. (2015) Advanced two-moment bulk microphysics for global models. Part II: Global model solutions and aerosol–cloud interactions. *Journal of Climate*, 28, 1288–1307. https://doi.org/10.1175/jcli-d-14-00103.1.

Gettelman, A., Truesdale, J.E., Bacmeister, J.T., Caldwell, P.M., Neale, R.B., Bogenschutz, P.A. and Simpson, I.R. (2019) The single column atmosphere model version 6 (SCAM6): not a SCAM but a tool for model evaluation and development. *Journal of Advances in Modeling Earth Systems*, 11, 1381–1401. https://doi.org/10.1029/2018ms001578.

Ghan, S., Randall, D., Xu, K.-.M., Cederwall, R., Cripe, D., Hack, J., Iacobellis, S., Klein, S., Krueger, S., Lohmann, U., Pedretti, J.A., Robock, A., Rotstayn, L., Somerville, R., Stenchikov, G., Sud, Y., Walker, G., Xie, S., Yio, J. and Zhang, M.H. (2000) A comparison of single column model simulations of summertime midlatitude continental convection. *Journal of Geophysical Research*, 105(D2), 2091–2124. https://doi.org/10.1029/1999JD900971.

Golaz, J.-C., Larson, V.E. and Cotton, W.R. (2002) A PDF-based model for boundary layer clouds. Part I: Method and model description. *Journal of the Atmospheric Sciences*, 59, 3540–3551. https://doi.org/10.1175/1520-0469(2002)059<3540:apbmfb>2.0.co;2.

Griffin, B.M. and Larson, V.E. (2016) Parameterizing microphysical effects on variances and covariances of moisture and heat content using a multivariate probability density function: a study with CLUBB (tag MVCS). *Geoscientific Model Development*, 9, 4273–4295. https://doi.org/10.5194/gmd-9-4273-2016.

Guichard, F., Petch, J.C., Redelsperger, J.-L., Bechtold, P., Chaboureau, J.-P., Cheinet, S., Grabowski, W., Grenier, H., Jones, C.G., Köhler, M., Piriou, J.-M., Tailleux, R. and Tomasini, M. (2004) Modelling the diurnal cycle of deep precipitating convection over land with cloud-resolving models and single-column models. *Quarterly Journal of the Royal Meteorological Society*, 130(604), 3139–3172. https://doi.org/10.1256/qj.03.145.

Guo, Z., Griffin, B.M., Domke, S. and Larson, V.E. (2021) A parameterization of turbulent dissipation and pressure damping time scales in stably stratified inversions, and its effects on low clouds in global simulations. *Journal of Advances in Modeling Earth Systems*, 13, e2020MS002278. https://doi.org/10.1029/2020MS002278.

Han, J.-Y., Hong, S.-Y. and Kwon, Y.C. (2020) The performance of a revised simplified Arakawa–Schubert (SAS) convection scheme in the medium-range forecasts of the Korean integrated model (KIM). *Weather and Forecasting*, 35, 1113–1128. https://doi.org/10.1175/waf-d-19-0219.1.

Han, J. and Pan, H.-L. (2011) Revision of convection and vertical diffusion schemes in the NCEP global forecast system. *Weather and Forecasting*, 26, 520–533. https://doi.org/10.1175/waf-d-10-05038.1.

Hohenegger, C. and Stevens, B. (2013) Preconditioning deep convection with cumulus congestus. *Journal of the Atmospheric Sciences*, 70, 448–464. https://doi.org/10.1175/jas-d-12-089.1.

Holloway, C.E. and Neelin, J.D. (2009) Moisture vertical structure, column water vapor, and tropical deep convection. *Journal of the Atmospheric Sciences*, 66, 1665–1683. https://doi.org/10.1175/2008jas2806.1.

Holtslag, A.A.M. and Boville, B.A. (1993) Local versus nonlocal boundary-layer diffusion in a global climate model. *Journal of Climate*, 6, 1825–1842. https://doi.org/10.1175/1520-0442(1993)006<1825:Lvnbld>2.0.Co;2.

Hong, S.-Y., Dudhia, J. and Chen, S.-H. (2004) A revised approach to ice microphysical processes for the bulk parameterization of clouds and precipitation. *Monthly Weather Review*, 132, 103–120. https://doi.org/10.1175/1520-0493(2004)132<0103:Aratim>2.0.Co;2.

Hong, S.-Y., Park, H., Cheong, H.-B., Kim, J.-E.E., Koo, M.-S., Jang, J., Ham, S., Hwang, S.-O., Park, B.-K., Chang, E.-C. and Li, H.Q. (2013) The global/regional integrated model system (GRIMs). *Asia-Pacific Journal of Atmospheric Sciences*, 49, 219–243. https://doi.org/10.1007/s13143-013-0023-0.

Hong, S.-Y., Kwon, Y.C., Kim, T.-H., Kim, J.-E.E., Choi, S.-J., Kwon, I.-H., Kim, J.H., Lee, E.-H., Park, R.-S. and Kim, D.-I. (2018) The Korean integrated model (KIM) system for global weather forecasting. *Asia-Pacific Journal of Atmospheric Sciences*, 54, 267–292. https://doi.org/10.1007/s13143-018-0028-9.

Jensen, M.P., Petersen, W.A., Bansemer, A., Bharadwaj, N., Carey, L.D., Cecil, D.J., Collis, S.M., Del Genio, A.D., Dolan, B., Gerlach, J., Giangrande, S.E., Heymsfield, A., Heymsfield, G., Kollias, P., Lang, T.J., Nesbitt, S.W., Neumann, A., Poellot, M., Rutledge, S.A., Schwaller, M., Tokay, A., Williams, C.R., Wolff, D.B., Xie, S. and Zipser, E.J. (2016) The Midlatitude Continental Convective Clouds Experiment (MC3E). *Bulletin of the American Meteorological Society*, 97, 1667–1686. https://doi.org/10.1175/bams-d-14-00228.1.

Kain, J.S. and Fritsch, J.M. (1990) A one-dimensional entraining/detraining plume model and its application in convective parameterization. *Journal of the Atmospheric Sciences*, 47, 2784–2802. https://doi.org/10.1175/1520-0469(1990)047<2784:Aodepm>2.0.Co;2.

Kain, J.S. and Fritsch, J.M. (1992) The role of the convective "trigger function" in numerical forecasts of mesoscale convective systems. *Meteorology and Atmospheric Physics*, 49, 93–106. https://doi.org/10.1007/BF01025402.

Khairoutdinov, M. and Randall, D. (2006) High-resolution simulation of shallow-to-deep convection transition over land. *Journal of the Atmospheric Sciences*, 63, 3421–3436. https://doi.org/10.1175/jas3810.1.

Khouider, B. and Leclerc, E. (2019) Toward a stochastic relaxation for the quasi-equilibrium theory of cumulus parameterization: multicloud instability, multiple equilibria, and chaotic dynamics. *Journal of Advances in Modeling Earth Systems*, 11, 2474–2502.

Kim, S.-Y. and Hong, S.-Y. (2018) The use of partial cloudiness in a bulk cloud microphysics scheme: concept and 2D results. *Journal of the Atmospheric Sciences*, 75, 2711–2719. https://doi.org/10.1175/jas-d-17-0234.1.

Klein, S.A., McCoy, R.B., Morrison, H., Ackerman, A.S., Avramov, A., de Boer, G., Chen, M.X., Cole, J.N.S., Del Genio, A.D., Falk, M., Foster, M.J., Fridlind, A., Golaz, J.-C., Hashino, T., Harrington, J.Y., Hoose, C., Khairoutdinov, M.F., Larson, V.E., Liu, X.H., Luo, Y.L., McFarquhar, G.M., Menon, S., Neggers, R.A.J., Park, S., Poellot, M.R., Schmidt, J.M., Sednev, I., Shipway, B.J., Shupe, M.D., Spangenberg, D.A., Sud, Y.C., Turner, D.D., Veron, D.E., von Salzen, K., Walker, G.K., Wang, Z., Wolf, A.B., Xie, S.C., Xu, K.-M., Yang, F.L. and Zhang, G. (2009) Intercomparison of model simulations of mixed-phase clouds observed during the ARM Mixed-Phase Arctic Cloud Experiment. I: Single-layer cloud. *Quarterly Journal of the Royal Meteorological Society*, 135(641), 979–1002. https://doi.org/10.1002/qj.416.

Köhler, M. (2020) Cloud cover. Chapter 3.8.5 in *ICON Tutorial: Working with the ICON Model*, F. Prill, D. Reinert, D. Rieger, and G. Zängl, November 2020. https://doi.org/10.5676/dwd_pub/nwv/icon_tutorial2020

Koo, M.-S. and Hong, S.-Y. (2010) Diurnal variations of simulated precipitation over East Asia in two regional climate models. *Journal of Geophysical Research*, 115, D05105. https://doi.org/10.1029/2009JD012574.

Koo, M.-S., Baek, S., Seol, K.-H. and Cho, K. (2017) Advances in land modeling of KIAPS based on the Noah land surface model. *Asia-Pacific Journal of Atmospheric Sciences*, 53, 361–373. https://doi.org/10.1007/s13143-017-0043-2.

Kuo, Y.-H., Schiro, K.A. and Neelin, J.D. (2018) Convective transition statistics over tropical oceans for climate model diagnostics: observational baseline. *Journal of the Atmospheric Sciences*, 75, 1553–1570. https://doi.org/10.1175/jas-d-17-0287.1.

Kuo, Y.-H., Ackerman, A.S., Angevine, W.M., Bazile, E., Beau, I., Blossey, P.N., Boutle, I.A., de Bruijn, C., Cheng, A., van der Dussen, J., Fletcher, J., Dal Gesso, S., Jam, A., Kawai, H., Cheedela, S.K., Larson, V.E., Lefebvre, M.P., Lock, A.P., Meyer, N.R. and de Roode, S.R. (2020) Convective transition statistics over tropical oceans for climate model diagnostics: GCM evaluation. *Journal of the Atmospheric Sciences*, 77, 379–403. https://doi.org/10.1175/jas-d-19-0132.1.

Larson, V.E. and Golaz, J.-C. (2005) Using probability density functions to derive consistent closure relationships among higher-order moments. *Monthly Weather Review*, 133, 1023–1042. https://doi.org/10.1175/mwr2902.1.

Larson, V.E. and Schanen, D.P. (2013) The subgrid importance Latin hypercube sampler (SILHS): a multivariate subcolumn generator. *Geoscientific Model Development*, 6, 1813–1829. https://doi.org/10.5194/gmd-6-1813-2013.

Larson, V.E. (2017) *CLUBB-SILHS: a parameterization of subgrid variability in the atmosphere*. ArXiv:1711.03675 [Physics].

Lawrence, D.M., Fisher, R.A., Koven, C.D., Oleson, K.W., Swenson, S.C., Bonan, G., Collier, N., Ghimire, B., van Kampenhout, L., Kennedy, D., Kluzek, E., Lawrence, P.J., Li, F., Li, H.Y., Lombardozzi, D., Riley, W.J., Sacks, W.J., Shi, M.J., Vertenstein, M., Wieder, W.R., Xu, C.G., Ali, A.A., Badger, A.M., Bisht, G., van den Broeke, M., Brunke, M.A., Burns, S.P., Buzan, J., Clark, M., Craig, A., Dahlin, K., Drewniak, B., Fisher, J.B., Flanner, M., Fox, A.M., Gentine, P., Hoffman, F., Keppel-Aleks, G., Knox, R., Kumar, S., Lenaerts, J., Leung, L.R., Lipscomb, W.H., Lu, Y.Q., Pandey, A., Pelletier, J.D., Perket, J., Randerson, J.T., Ricciuto, D.M., Sanderson, B.M., Slater, A., Subin, Z.M., Tang, J.Y., Thomas, R.Q., Martin, M.V. and Zeng, X.B. (2019) The community land model version 5: description of new features, benchmarking, and impact of forcing uncertainty. *Journal of Advances in Modeling Earth Systems*, 11, 4245–4287. https://doi.org/10.1029/2018MS001583.

Lee, E.-H., Lee, E., Park, R., Kwon, Y.C. and Hong, S.-Y. (2018) Impact of turbulent mixing in the stratocumulus-topped boundary layer on numerical weather prediction. *Asia-Pacific Journal of Atmospheric Sciences*, 54, 371–384. https://doi.org/10.1007/s13143-018-0024-0.

Lee, M.-I., Schubert, S.D., Suarez, M.J., Schemm, J.-K.E., Pan, H.-L., Han, J. and Yoo, S.-H. (2008) Role of convection triggers in the simulation of the diurnal cycle of precipitation over the United States Great Plains in a general circulation model. *Journal of Geophysical Research*, 113, D02111. https://doi.org/10.1029/2007JD008984.

Lee, W.L., Wang, Y.-C., Shiu, C.-J., Tsai, I.-C., Tu, C.-Y., Lan, Y.-Y., Chen, J.-P., Pan, H.-L. and Hsu, H.-H. (2020) Taiwan Earth system model version 1: description and evaluation of mean state. *Geoscientific Model Development Discussion*, 2020, 1–43. https://doi.org/10.5194/gmd-2019-377.

Lenderink, G., Siebesma, A.P., Cheinet, S., Irons, S., Jones, C.G., Marquet, P., Müller, F., Olmeda, D., Calvo, J., Sánchez, E. and Soares, P.M.M. (2004) The diurnal cycle of shallow cumulus clouds over land: a single-column model intercomparison study. *Quarterly Journal of the Royal Meteorological Society*, 130(604), 3339–3364. https://doi.org/10.1256/qj.03.122.

Ma, H.-Y., Zhang, K., Tang, S., Xie, S. and Fu, R. (2021a) Evaluation of the causes of wet-season dry biases over Amazonia in CAM5. *Journal of Geophysical Research: Atmospheres*, 126(11), e2020JD033859. https://doi.org/10.1029/2020JD033859.

Ma, H.Y., Zhou, C., Zhang, Y.Y., Klein, S.A., Zelinka, M.D., Zheng, X., Xie, S.C., Chen, W.-T. and Wu, C.-M. (2021b) A multi-year short-range hindcast experiment with CESM1 for evaluating climate model moist processes from diurnal to interannual timescales. *Geoscientific Model Development*, 14, 73–90. https://doi.org/10.5194/gmd-14-73-2021.

Malardel, S. and Bechtold, P. (2019) The coupling of deep convection with the resolved flow via the divergence of mass flux in the IFS. *Quarterly Journal of the Royal Meteorological Society*, 145(722), 1832–1845. https://doi.org/10.1002/qj.3528.

Mapes, B. and Neale, R. (2011) Parameterizing convective organization to escape the entrainment dilemma. *Journal of Advances in Modeling Earth Systems*, 3, M06004. https://doi.org/10.1029/2011MS000042.

Martin, S.T., Artaxo, P., Machado, L.A.T., Manzi, A.O., Souza, R.A.F., Schumacher, C., Wang, J., Andreae, M.O., Barbosa, H.M.J., Fan, J., Fisch, G., Goldstein, A.H., Guenther, A., Jimenez, J.L., Pöschl, U., Dias, M.A.S., Smith, J.N. and Wendisch, M. (2016) Introduction: observations and modeling of the Green Ocean Amazon (GoAmazon2014/5). *Atmospheric Chemistry and Physics*, 16, 4785–4797. https://doi.org/10.5194/acp-16-4785-2016.

McTaggart-Cowan, R., Vaillancourt, P.A., Zadra, A., Chamberland, S., Charron, M., Corvec, S., Milbrandt, J.A., Paquin-Ricard, D., Patoine, A., Roch, M., Separovic, L. and Yang, J. (2019a) Modernization of atmospheric physics parameterization in Canadian NWP. *Journal of Advances in Modeling Earth Systems*, 11, 3593–3635. https://doi.org/10.1029/2019ms001781.

McTaggart-Cowan, R., Vaillancourt, P.A., Zadra, A., Separovic, L., Corvec, S. and Kirshbaum, D. (2019b) A Lagrangian perspective on parameterizing deep convection. *Monthly Weather Review*, 147, 4127–4149. https://doi.org/10.1175/mwr-d-19-0164.1.

McTaggart-Cowan, R., Vaillancourt, P.A., Separovic, L., Corvec, S. and Zadra, A. (2020) A convection parameterization for low-CAPE environments. *Monthly Weather Review*, 148, 4917–4941. https://doi.org/10.1175/mwr-d-20-0020.1.

Morrison, H. and Gettelman, A. (2008) A new two-moment bulk stratiform cloud microphysics scheme in the Community Atmosphere Model, version 3 (CAM3). Part I: Description and numerical tests. *Journal of Climate*, 21, 3642–3659. https://doi.org/10.1175/2008JCLI2105.1.

Morrison, H., McCoy, R.B., Klein, S.A., Xie, S.C., Luo, Y.L., Avramov, A., Chen, M.X., Cole, J.N.S., Falk, M., Foster, M.J., Del Genio, A.D., Harrington, J.Y., Hoose, C., Khairoutdinov, M.F., Larson, V.E., Liu, X.H., McFarquhar, G.M., Poellot, M.R., von Salzen, K., Shipway, B.J., Shupe, M.D., Sud, Y.C., Turner, D.D., Veron, D.E., Walker, G.K., Wang, Z., Wolf, A.B., Xu, K.-M., Yang, F.L. and Zhang, G. (2009) Intercomparison of model simulations of mixed-phase clouds observed during the ARM Mixed-Phase Arctic Cloud Experiment. II: Multilayer cloud. *Quarterly Journal of the Royal Meteorological Society*, 135(641), 1003–1019. https://doi.org/10.1002/qj.415.

Neale, R.B., Richter, J.H., Conley, A.J., Park, S., Lauritzen, P.H., Gettelman, A. and Williamson, D.L. (2012) *Description of the NCAR Community Atmosphere Model (CAM 5.0)*. NCAR Technical Note NCARTN-4861STR, pp 274.

Neelin, J.D., Peters, O. and Hales, K. (2009) The transition to strong convection. *Journal of the Atmospheric Sciences*, 66, 2367–2384. https://doi.org/10.1175/2009jas2962.1.

Neggers, R.A.J., Siebesma, A.P. and Heus, T. (2012) Continuous single-column model evaluation at a permanent meteorological supersite. *Bulletin of the American Meteorological Society*, 93, 1389–1400. https://doi.org/10.1175/bams-d-11-00162.1.

Neggers, R.A.J. and Siebesma, A.P. (2013) Constraining a system of interacting parameterizations through multiple-parameter evaluation: tracing a compensating error between cloud vertical structure and cloud overlap. *Journal of Climate*, 26, 6698–6715. https://doi.org/10.1175/jcli-d-12-00779.1.

Neggers, R.A.J. (2015a) Exploring bin-macrophysics models for moist convective transport and clouds. *Journal of Advances in Modeling Earth Systems*, 7, 2079–2104. https://doi.org/10.1002/2015ms000502.

Neggers, R.A.J. (2015b) Attributing the behavior of low-level clouds in large-scale models to subgrid-scale parameterizations. *Journal of Advances in Modeling Earth Systems*, 7, 2029–2043. https://doi.org/10.1002/2015MS000503.

Neggers, R.A.J., Ackerman, A.S., Angevine, W.M., Bazile, E., Beau, I., Blossey, P.N., Boutle, I.A., de Bruijn, C., Cheng, A., van der Dussen, J., Fletcher, J., Dal Gesso, S., Jam, A., Kawai, H., Cheedela, S.K., Larson, V.E., Lefebvre, M.P., Lock, A.P., Meyer, N.R. and de Roode, S.R. (2017) Single-column model simulations of subtropical marine boundary-layer cloud transitions under weakening inversions. *Journal of Advances in Modeling Earth Systems*, 9, 2385–2412. https://doi.org/10.1002/2017MS001064.

Oliveira, M.I., Acevedo, O.C., Sörgel, M., Nascimento, E.L., Manzi, A.O., Oliveira, P.E.S., Brondani, D.V., Tsokankunku, A. and Andreae, M.O. (2020) Planetary boundary layer evolution over the Amazon rainforest in episodes of deep moist convection at the Amazon tall tower observatory. *Atmospheric Chemistry and Physics*, 20, 15–27. https://doi.org/10.5194/acp-20-15-2020.

Park, R.-S., Chae, J.-H. and Hong, S.-Y. (2016) A revised prognostic cloud fraction scheme in a global forecasting system. *Monthly Weather Review*, 144, 1219–1229. https://doi.org/10.1175/mwr-d-15-0273.1.

Park, S. and Bretherton, C.S. (2009) The University of Washington shallow convection and moist turbulence schemes and their impact on climate simulations with the community atmosphere model. *Journal of Climate*, 22, 3449–3469. https://doi.org/10.1175/2008JCLI2557.1.

Park, S. (2014a) A unified convection scheme (UNICON). Part I: Formulation. *Journal of the Atmospheric Sciences*, 71, 3902–3930. https://doi.org/10.1175/jas-d-13-0233.1.

Park, S. (2014b) A unified convection scheme (UNICON). Part II: Simulation. *Journal of the Atmospheric Sciences*, 71, 3931–3973. https://doi.org/10.1175/jas-d-13-0234.1.

Park, S., Bretherton, C.S. and Rasch, P.J. (2014) Integrating cloud processes in the community atmosphere model, version 5. *Journal of Climate*, 27, 6821–6856. https://doi.org/10.1175/JCLI-D-14-00087.1.

Park, S., Baek, E.-H., Kim, B.-M. and Kim, S.-J. (2017) Impact of detrained cumulus on climate simulated by the community atmosphere model version 5 with a unified convection scheme. *Journal of Advances in Modeling Earth Systems*, 9, 1399–1411. https://doi.org/10.1002/2016MS000877.

Park, S., Shin, J., Kim, S., Oh, E. and Kim, Y. (2019) Global climate simulated by the Seoul National University atmosphere model version 0 with a unified convection scheme (SAM0-UNICON). *Journal of Climate*, 32, 2917–2949. https://doi.org/10.1175/jcli-d-18-0796.1.

Petch, J., Hill, A., Davies, L., Fridlind, A., Jakob, C., Lin, Y.L., Xie, S.C. and Zhu, P. (2014) Evaluation of intercomparisons of four different types of model simulating TWP-ICE. *Quarterly Journal of the Royal Meteorological Society*, 140(680), 826–837. https://doi.org/10.1002/qj.2192.

Pithan, F., Ackerman, A., Angevine, W.M., Hartung, K., Ickes, L., Kelley, M., Medeiros, B., Sandu, I., Steeneveld, G.-J., Sterk, H.A.M., Svensson, G., Vaillancourt, P.A. and Zadra, A. (2016) Select strengths and biases of models in representing the Arctic winter boundary layer over sea ice: the Larcform 1 single column model intercomparison. *Journal of Advances in Modeling Earth Systems*, 8, 1345–1357. https://doi.org/10.1002/2016MS000630.

Randall, D.A., Xu, K.-M., Somerville, R.J.C. and Iacobellis, S. (1996) Single-column models and cloud ensemble models as links between observations and climate models. *Journal of Climate*, 9, 1683–1697. https://doi.org/10.1175/1520-0442(1996)009<1683:SCMACE>2.0.CO;2.

Rasch, P.J., Xie, S., Ma, P.-L., Lin, W., Wang, H., Tang, Q., Burrows, S.M., Caldwell, P., Zhang, K., Easter, R.C., Cameron-Smith, P., Singh, B., Wan, H., Golaz, J.-C., Harrop, B.E., Roesler, E., Bacmeister, J., Larson, V.E., Evans, K.J., Qian, Y., Taylor, M., Leung, L.R., Zhang, Y., Brent, L., Branstetter, M., Hannay, C., Mahajan, S., Mametjanov, A., Neale, R., Richter, J.H., Yoon, J.-H., Zender, C.S., Bader, D., Flanner, M., Foucar, J.G., Jacob, R., Keen, N., Klein, S.A., Liu, X., Salinger, A.G., Shrivastava, M. and Yang, Y. (2019) An overview of the atmospheric component of the energy exascale Earth system model. *Journal of Advances in Modeling Earth Systems*, 11, 2377–2411. https://doi.org/10.1029/2019ms001629.

Raschendorfer, M. (2000) The new turbulence parameterization in the Lokal-Modell of DWD. *Research Activities in Atmospheric and Oceanic Modelling*. WMO/TD-No. 987, pp. 4.30–4.31.

Rio, C., Hourdin, F., Grandpeix, J.Y. and Lafore, J.P. (2009) Shifting the diurnal cycle of parameterized deep convection over land. *Geophysical Research Letters*, 36(7), L07809. https://doi.org/10.1029/2008GL036779.

Rio, C., Grandpeix, J.-Y., Hourdin, F., Guichard, F., Couvreux, F., Lafore, J.-P., Fridlind, A., Mrowiec, A., Roehrig, R., Rochetin, N., Lefebvre, M.-P. and Idelkadi, A. (2013) Control of deep convection by sub-cloud lifting processes: the ALP closure in the LMDZ5B general circulation model. *Climate Dynamics*, 40, 2271–2292. https://doi.org/10.1007/s00382-012-1506-x.

Ruppert, J.H. and Johnson, R.H. (2015) Diurnally modulated cumulus moistening in the preonset stage of the Madden–Julian Oscillation during DYNAMO. *Journal of the Atmospheric Sciences*, 72, 1622–1647. https://doi.org/10.1175/JAS-D-14-0218.1.

Rutledge, S.A. and Hobbs, P.V. (1984) The mesoscale and microscale structure and organization of clouds and precipitation in midlatitude cyclones. XII: A diagnostic modeling study of precipitation development in narrow cold-frontal rainbands. *Journal of the Atmospheric Sciences*, 41, 2949–2972. https://doi.org/10.1175/1520-0469(1984)041<2949:Tmamsa>2.0.Co;2.

Schumacher, C., Houze Jr, R.A. and Kraucunas, I. (2004) The tropical dynamical response to latent heating estimates derived from the TRMM precipitation radar. *Journal of the Atmospheric Sciences*, 61, 1341–1358. https://doi.org/10.1175/1520-0469(2004)061<1341:TTDRTL>2.0.CO;2.

Seifert, A. (2008) A revised cloud microphysical parameterization for COSMO-LME. *COSMO Newsletter*, 7, 25–28.

Shin, H.H. and Hong, S.-Y. (2015) Representation of the subgrid-scale turbulent transport in convective boundary layers at gray-zone resolutions. *Monthly Weather Review*, 143, 250–271. https://doi.org/10.1175/mwr-d-14-00116.1.

Shiu, C.J., Wang, Y.-C., Hsu, H.-H., Chen, W.-T., Pan, H.-L., Sun, R.Y., Chen, Y.-H. and Chen, C.-A. (2021) GTS v1.0: a macrophysics scheme for climate models based on a probability density function. *Geoscientific Model Development*, 14, 177–204. https://doi.org/10.5194/gmd-14-177-2021.

Stephens, G.L., L'Ecuyer, T., Forbes, R., Gettelmen, A., Golaz, J.-C., Bodas-Salcedo, A., Suzuki, K., Gabriel, P. and Haynes, J. (2010) Dreary state of precipitation in global models. *Journal of Geophysical Research*, 115, D24211. https://doi.org/10.1029/2010JD014532.

Stratton, R.A. and Stirling, A.J. (2012) Improving the diurnal cycle of convection in GCMs. *Quarterly Journal of the Royal Meteorological Society*, 138(666), 1121–1134. https://doi.org/10.1002/qj.991.

Sun, Y., Solomon, S., Dai, A. and Portmann, R.W. (2007) How often will it rain? *Journal of Climate*, 20, 4801–4818. https://doi.org/10.1175/jcli4263.1.

Sundqvist, H., Berge, E. and Kristjánsson, J.E. (1989) Condensation and cloud parameterization studies with a mesoscale numerical weather prediction model. *Monthly Weather Review*, 117, 1641–1657. https://doi.org/10.1175/1520-0493(1989)117<1641:Cacpsw>2.0.Co;2.

Tang, S., Xie, S.C., Zhang, Y.Y., Zhang, M.H., Schumacher, C., Upton, H., Jensen, M.P., Johnson, K.L., Wang, M., Ahlgrimm, M., Feng, Z., Minnis, P. and Thieman, M. (2016) Large-scale vertical velocity, diabatic heating and drying profiles associated with seasonal and diurnal variations of convective systems observed in the GoAmazon2014/5 experiment. *Atmospheric Chemistry and Physics*, 16, 14249–14264. https://doi.org/10.5194/acp-16-14249-2016.

Tang, S., Xie, S.C., Zhang, M.H., Tang, Q., Zhang, Y.Y., Klein, S.A., Cook, D.R. and Sullivan, R.C. (2019) Differences in eddy-correlation and energy-balance surface turbulent heat flux measurements and their impacts on the large-scale forcing fields at the ARM SGP site. *Journal of Geophysical*

Research – Atmospheres, 124, 3301–3318. https://doi.org/10.1029/2018jd029689.

Tang, S., Gleckler, P., Xie, S., Lee, J., Ahn, M.-S., Covey, C. and Zhang, C. (2021) Evaluating the diurnal and semidiurnal cycle of precipitation in CMIP6 models using satellite- and ground-based observations. *Journal of Climate*, 34, 3189–3210. https://doi.org/10.1175/jcli-d-20-0639.1.

Taylor, K.E., Stouffer, R.J. and Meehl, G.A. (2012) An overview of CMIP5 and the experiment design. *Bulletin of the American Meteorological Society*, 93, 485–498. https://doi.org/10.1175/bams-d-11-00094.1.

Thayer-Calder, K., Gettelman, A., Craig, C., Goldhaber, S., Bogenschutz, P.A., Chen, C.-C., Morrison, H., Höft, J., Raut, E., Griffin, B.M., Weber, J.K., Larson, V.E., Wyant, M.C., Wang, M., Guo, Z. and Ghan, S.J. (2015) A unified parameterization of clouds and turbulence using CLUBB and subcolumns in the community atmosphere model. *Geoscientific Model Development*, 8, 3801–3821. https://doi.org/10.5194/gmd-8-3801-2015.

Tian, Y., Zhang, Y., Klein, S.A. and Schumacher, C. (2021) Interpreting the diurnal cycle of clouds and precipitation in the ARM GoAmazon observations: shallow to deep convection transition. *Journal of Geophysical Research – Atmospheres*, 126, e2020JD033766. https://doi.org/10.1029/2020JD033766.

Trenberth, K.E., Dai, A., Rasmussen, R.M. and Parsons, D.B. (2003) The changing character of precipitation. *Bulletin of the American Meteorological Society*, 84, 1205–1218. https://doi.org/10.1175/bams-84-9-1205.

Varble, A.C., Nesbitt, S.W., Salio, P., Hardin, J.C., Bharadwaj, N., Borque, P., DeMott, P.J., Feng, Z., Hill, T.C.J., Marquis, J.N., Matthews, A., Mei, F., Öktem, R., Castro, V., Goldberger, L., Hunzinger, A., Barry, K.R., Kreidenweis, S.M., McFarquhar, G.M., McMurdie, L.A., Pekour, M., Powers, H., Romps, D.M., Saulo, C., Schmid, B., Tomlinson, J.M., van den Heever, S.C., Zelenyuk, A., Zhang, Z.X. and Zipser, E.J. (2021) Utilizing a storm-generating hotspot to study convective cloud transitions: the CACTI experiment. *Bulletin of the American Meteorological Society*, 102, E1597–E1620. https://doi.org/10.1175/bams-d-20-0030.1.

Wang, Y.-C. and Hsu, H.-H. (2019) Improving diurnal rainfall phase over the southern Great Plains in warm seasons by using a convective triggering design. *International Journal of Climatology*, 39, 5181–5190. https://doi.org/10.1002/joc.6117.

Wang, Y.-C., Xie, S., Tang, S. and Lin, W. (2020) Evaluation of an improved convective triggering function: observational evidence and SCM tests. *Journal of Geophysical Research – Atmospheres*, 125, e2019JD031651. https://doi.org/10.1029/2019jd031651.

Wang, Y., Zhou, L. and Hamilton, K. (2007) Effect of convective entrainment/detrainment on the simulation of the tropical precipitation diurnal cycle. *Monthly Weather Review*, 135, 567–585. https://doi.org/10.1175/mwr3308.1.

Wang, Y.C., Pan, H.L. and Hsu, H.H. (2015) Impacts of the triggering function of cumulus parameterization on warm-season diurnal rainfall cycles at the atmospheric radiation measurement southern Great Plains site. *Journal of Geophysical Research: Atmospheres*, 120, 10681–10702. https://doi.org/10.1002/2015JD023337.

Wei, Y., Pu, Z. and Zhang, C. (2020) Diurnal cycle of precipitation over the maritime continent under modulation of MJO: perspectives from cloud-permitting scale simulations. *Journal of Geophysical Research – Atmospheres*, 125, e2020JD032529. https://doi.org/10.1029/2020JD032529.

Wyant, M.C., Bretherton, C.S., Chlond, A., Griffin, B.M., Kitagawa, H., Lappen, C.-L., Larson, V.E., Lock, A., Park, S.S., de Roode, S.R., Uchida, J., Zhao, M. and Ackerman, A.S. (2007) A single-column model intercomparison of a heavily drizzling stratocumulus-topped boundary layer. *Journal of Geophysical Research*, 112, D24204. https://doi.org/10.1029/2007jd008536.

Xie, S. and Zhang, M. (2000) Impact of the convection triggering function on single-column model simulations. *Journal of Geophysical Research*, 105(D11), 14983–14996. https://doi.org/10.1029/2000JD900170.

Xie, S., Xu, K.-M., Cederwall, R.T., Bechtold, P., Del Genio, A.D., Klein, S.A., Cripe, D.G., Ghan, S.J., Gregory, D., Iacobellis, S.F., Krueger, S.K., Lohmann, U., Petch, J.C., Randall, D.A., Rotstayn, L.D., Somerville, R.C.J., Sud, Y.C., Von Salzen, K., Walker, G.K. and Wolf, A. (2002) Intercomparison and evaluation of cumulus parametrizations under summertime midlatitude continental conditions. *Quarterly Journal of the Royal Meteorological Society*, 128(582), 1095–1135. https://doi.org/10.1256/003590002320373229.

Xie, S., Cederwall, R.T. and Zhang, M. (2004) Developing long-term single-column model/cloud system–resolving model forcing data using numerical weather prediction products constrained by surface and top of the atmosphere observations. *Journal of Geophysical Research*, 109, D01104. https://doi.org/10.1029/2003jd004045.

Xie, S., Zhang, M.H., Branson, M., Cederwall, R.T., Del Genio, A.D., Eitzen, Z.A., Ghan, S.J., Iacobellis, S.F., Johnson, K.L., Khairoutdinov, M., Klein, S.A., Krueger, S.K., Lin, W.Y., Lohmann, U., Miller, M.A., Randall, D.A., Somerville, R.C.J., Sud, Y.C., Walker, G.K. and Wolf, A. (2005) Simulations of midlatitude frontal clouds by single-column and cloud-resolving models during the Atmospheric Radiation Measurement March 2000 cloud intensive operational period. *Journal of Geophysical Research*, 110(D15), D15S03. https://doi.org/10.1029/2004JD005119.

Xie, S., Lin, W.Y., Rasch, P.J., Ma, P.-L., Neale, R., Larson, V.E., Qian, Y., Bogenschutz, P.A., Caldwell, P., Cameron-Smith, P., Golaz, J.-C., Mahajan, S., Singh, B., Tang, Q., Wang, H.L., Yoon, J.-H., Zhang, K. and Zhang, Y.Y. (2018) Understanding cloud and convective characteristics in version 1 of the E3SM atmosphere model. *Journal of Advances in Modeling Earth Systems*, 10, 2618–2644. https://doi.org/10.1029/2018MS001350.

Xie, S., Wang, Y.-C., Lin, W.Y., Ma, H.-Y., Tang, Q., Tang, S.Q., Zheng, X., Golaz, J.-C., Zhang, G.J. and Zhang, M.H. (2019) Improved diurnal cycle of precipitation in E3SM with a revised convective triggering function. *Journal of Advances in Modeling Earth Systems*, 11, 2290–2310. https://doi.org/10.1029/2019ms001702.

Xu, K.-M., Zhang, M.H., Eitzen, Z., Ghan, S., Klein, S., Wu, X.Q., Xie, S., Branson, M., Genio, A., Iacobellis, S., Khairoutdinov, M., Lin, W.Y., Lohmann, U., Randall, D., Somerville, R., Sud, Y., Walker, G., Wolf, A., Yio, J. and Zhang, J.H. (2005) Modeling springtime shallow frontal clouds with cloud-resolving and single-column models. *Journal of Geophysical Research*, 110, D15S04. https://doi.org/10.1029/2004JD005153.

Yanai, M., Esbensen, S. and Chu, J.-H. (1973) Determination of bulk properties of tropical cloud clusters from large-scale heat and moisture budgets. *Journal of the Atmospheric Sciences*, 30, 611–627. https://doi.org/10.1175/1520-0469(1973)030<0611:DOBPOT>2.0.CO;2.

Zängl, G., Reinert, D., Rípodas, P. and Baldauf, M. (2015) The ICON (ICOsahedral Non-hydrostatic) modelling framework of DWD and MPI-M: description of the non-hydrostatic dynamical core. *Quarterly Journal of the Royal Meteorological Society*, 141(687), 563–579. https://doi.org/10.1002/qj.2378.

Zermeño-Díaz, D.M., Zhang, C., Kollias, P. and Kalesse, H. (2015) The role of shallow cloud moistening in MJO and non-MJO convective events over the ARM Manus site. *Journal of the Atmospheric Sciences*, 72, 4797–4820. https://doi.org/10.1175/JAS-D-14-0322.1.

Zhang, G.J. and McFarlane, N.A. (1995) Sensitivity of climate simulations to the parameterization of cumulus convection in the Canadian climate centre general circulation model. *Atmosphere–Ocean*, 33, 407–446. https://doi.org/10.1080/07055900.1995.9649539.

Zhang, G.J. (2003) Roles of tropospheric and boundary layer forcing in the diurnal cycle of convection in the US southern Great Plains. *Geophysical Research Letters*, 30, 2281. https://doi.org/10.1029/2003GL018554.

Zhang, M. and Lin, J. (1997) Constrained variational analysis of sounding data based on column-integrated budgets of mass, heat, moisture, and momentum: approach and application to ARM measurements. *Journal of the Atmospheric Sciences*, 54, 1503–1524. https://doi.org/10.1175/1520-0469(1997)054<1503:CVAOSD>2.0.CO;2.

Zhang, M., Lin, J., Cederwall, R.T., Yio, J.J. and Xie, S.C. (2001) Objective analysis of ARM IOP data: method and sensitivity. *Monthly Weather Review*, 129, 295–311. https://doi.org/10.1175/1520-0493(2001)129<0295:OAOAID>2.0.CO;2.

Zhang, M., Somerville, R.C.J. and Xie, S. (2016) The SCM concept and creation of ARM forcing datasets. *Meteorological Monographs*, 57, 24.1–24.12. https://doi.org/10.1175/AMSMONOGRAPHS-D-15-0040.1.

Zhang, Y. and Klein, S.A. (2010) Mechanisms affecting the transition from shallow to deep convection over land: inferences from observations of the diurnal cycle collected at the ARM southern Great Plains site. *Journal of the Atmospheric Sciences*, 67, 2943–2959. https://doi.org/10.1175/2010JAS3366.1.

Zhu, P., Bretherton, C.S., Köhler, M., Cheng, A., Chlond, A., Geng, Q.Z., Austin, P., Golaz, J.-C., Lenderink, G., Lock, A. and Stevens, B. (2005) Intercomparison and interpretation of single-column model simulations of a nocturnal stratocumulus-topped marine boundary layer. *Monthly Weather Review*, 133, 2741–2758. https://doi.org/10.1175/mwr2997.1.

How to cite this article: (2021) Long-term single-column model intercomparison of diurnal cycle of precipitation over midlatitude and tropical land. *Quarterly Journal of the Royal Meteorological Society*, 1–29. Available from: https://doi.org/10.1002/qj.4222

APPENDIX

Model schemes and abbreviations in Tables 1–3

Bechtold14: convective scheme from Bechtold *et al.* (2014).

CAPE: convective available potential energy.

CIN: convective inhibition.

CLUBB: Cloud Layers Unified By Binormals (Golaz *et al.*, 2002; Larson and Golaz, 2005; Larson, 2017).

dCAPE: dynamic CAPE generation rate from large-scale tendency (Xie and Zhang, 2000).

UW-diag_TKE: University of Washington diagnostic turbulent kinetic energy scheme (Bretherton and Park, 2009).

GTS: Global Forecast System (GFS) – Taiwan Earth System Model (TaiESM) – Sundqvist scheme (Shiu *et al.*, 2021).

HanPan: shallow convection from Han and Pan (2011).

HB: turbulent scheme from Holtslag and Boville (1993).

Köhler20: cloud cover parametrization from Köhler (2020).

KSAS: Korean Integrated Model (KIM: Hong *et al.*, 2018) version of the simplified Arakawa–Schubert deep convection scheme (Han *et al.*, 2020).

LCL: lifting condensation level.

LFC: level of free convection.

M-Bechtold: modified from Bechtold *et al.* (2001) (McTaggart-Cowan *et al.*, 2019a).

MG: bulk two-moment cloud microphysics (Morrison and Gettelman, 2008).

MG2: version 2 of MG microphysics (Gettelman *et al.*, 2015).

Modified KF: modified from Kain and Fritsch (1990) (McTaggart-Cowan *et al.*, 2019a).

Park1: macrophysics from Park *et al.* (2014).

Park2: macrophysics from Park *et al.* (2017).

PCH16: macrophysics from Park *et al.* (2016).

UW-PB09: University of Washington shallow convective scheme (Park and Bretherton, 2009).

PBL: planetary boundary layer.

Raschendorfer00: turbulence scheme from Raschendorfer (2000).

Seifert08: single-moment microphysics from Seifert (2008).

Shin–Hong: turbulence scheme from Shin and Hong (2015) with revision of Lee *et al.* (2018).

SILHS: Subgrid Importance Latin Hypercube Sampler (Thayer-Calder *et al.*, 2015; Griffin and Larson, 2016).

Sundqvist: microphysics from Sundqvist *et al.* (1989).

TKE1.5: 1.5-order turbulent kinetic energy scheme from McTaggart-Cowan *et al.* (2019a).

UNICON: Unified convective scheme (Park, 2014a; 2014b).

Unified stochastic Plume-ZM: Unified Stochastic Mass-flux Cumulus integrated in ZM scheme (Khouider and Leclerc, 2019).

WSM5: the Weather Research and Forecasting (WRF) single-moment 5-class microphysics scheme (Hong *et al.*, 2004; Bae *et al.*, 2016; Kim and Hong, 2018).

ZM: Zhang–McFarlane convective scheme (Zhang and McFarlane, 1995).